



RESEARCH ARTICLE

10.1029/2024MS004342

Coupling Remote Sensing With a Process Model for the Simulation of Rangeland Carbon Dynamics

Key Points:

- The Rangeland Carbon Tracking and Monitoring System was calibrated to simulate vegetation type-specific rangeland C dynamics
- Regional variability in carbon fluxes and soil organic carbon is well represented by a remote sensing-driven process modeling approach
- Soil organic carbon stocks in Western and Midwestern US rangelands increased over the past 20 years due to increased precipitation

Supporting Information:

Supporting Information may be found in the online version of this article.

Correspondence to:

Y. Xia,
yushuxia@ldeo.columbia.edu

Citation:

Xia, Y., Sanderman, J., Watts, J. D., Machmuller, M. B., Mullen, A. L., Rivard, C., et al. (2025). Coupling remote sensing with a process model for the simulation of rangeland carbon dynamics. *Journal of Advances in Modeling Earth Systems*, 17, e2024MS004342. <https://doi.org/10.1029/2024MS004342>



















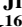

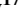

Received 28 MAR 2024

Accepted 25 FEB 2025

Author Contributions:

Conceptualization: Yushu Xia, Jonathan Sanderman, Jennifer D. Watts, Megan B. Machmuller, Andrew L. Mullen, Charlotte Rivard, John Kimball, Stephanie A. Ewing

Data curation: Yushu Xia, Jonathan Sanderman, Jennifer D. Watts, Megan B. Machmuller, Andrew L. Mullen, Charlotte Rivard, Arthur Endsley, Haydee Hernandez, Marcy Litvak, Tomer Duman, Praveena Krishnan, Tilden Meyers, Nathaniel A. Brunsell, Binayak Mohanty, Heping Liu,

Yushu Xia^{1,2} , Jonathan Sanderman¹, Jennifer D. Watts^{1,3} , Megan B. Machmuller⁴, Andrew L. Mullen¹, Charlotte Rivard^{1,5} , Arthur Endsley⁶ , Haydee Hernandez^{1,7}, John Kimball⁶ , Stephanie A. Ewing³ , Marcy Litvak⁸ , Tomer Duman⁸ , Praveena Krishnan⁹ , Tilden Meyers⁹, Nathaniel A. Brunsell¹⁰ , Binayak Mohanty¹¹, Heping Liu¹² , Zhongming Gao^{12,13} , Jiquan Chen¹⁴ , Michael Abraha¹⁴, Russell L. Scott¹⁵ , Gerald N. Flerchinger¹⁶, Patrick E. Clark¹⁶ , Paul C. Stoy¹⁷ , Anam M. Khan¹⁸ , E. N. Jack Brookshire³ , Quan Zhang^{19,20} , David R. Cook²¹, Thomas Thienelt²², Bhaskar Mitra²³ , Marguerite Mauritz-Tozer²⁴ , Craig E. Tweedie²⁴, Margaret S. Torn²⁵ , and Dave Billesbach²⁶

¹Woodwell Climate Research Center, Falmouth, MA, USA, ²Lamont Doherty Earth Observatory, Columbia University, Palisades, NY, USA, ³Department of Land Resources and Environmental Sciences, Montana State University, Bozeman, MT, USA, ⁴Natural Resources and Ecology Laboratory, Colorado State University, Fort Collins, CO, USA, ⁵Now at Center for Sustainable Development, The Brookings Institution, Washington, DC, USA, ⁶WA Franke College of Forestry and Conservation, The University of Montana, Missoula, MT, USA, ⁷Now at The Nature Conservancy, Colorado Field Office, Boulder, CO, USA, ⁸Department of Biology, University of New Mexico, Albuquerque, NM, USA, ⁹Atmospheric Turbulence and Diffusion Division, National Oceanic and Atmospheric Administration, Oak Ridge, TN, USA, ¹⁰Department of Geography and Atmospheric Science, University of Kansas, Lawrence, KS, USA, ¹¹Biological and Agricultural Engineering Department, Texas A&M University, College Station, TX, USA, ¹²Department of Civil and Environmental Engineering, Washington State University, Pullman, WA, USA, ¹³Now at School of Atmospheric Sciences, Sun Yat-sen University, Zhuhai, China, ¹⁴Department of Geography, Environment, and Spatial Sciences, Michigan State University, East Lansing, MI, USA, ¹⁵Southwest Watershed Research Center, USDA Agricultural Research Service, Tucson, AZ, USA, ¹⁶Northwest Watershed Research Center, USDA Agricultural Research Service, Boise, ID, USA, ¹⁷Department of Biological Systems Engineering, University of Wisconsin-Madison, Madison, WI, USA, ¹⁸Department of Forest and Wildlife Ecology, University of Wisconsin-Madison, Madison, WI, USA, ¹⁹School of Public and Environmental Affairs, Indiana University, Indianapolis, IN, USA, ²⁰Now at State Key Laboratory of Water Resources Engineering and Management, Wuhan University, Wuhan, China, ²¹Division of Environmental Science, Argonne National Laboratory, Lemont, IL, USA, ²²Department of Geoecology, Martin Luther University Halle-Wittenberg, Wittenberg, Germany, ²³Information and Computational Science, James Hutton Institute, Aberdeen, UK, ²⁴Department of Biological Sciences, The University of Texas at El Paso, El Paso, TX, USA, ²⁵Climate and Ecosystem Sciences Division, Lawrence Berkeley National Laboratory, Berkeley, CA, USA, ²⁶Department of Biological Systems Engineering, University of Nebraska-Lincoln, Lincoln, NE, USA

Abstract Rangelands provide significant environmental benefits through many ecosystem services, which may include soil organic carbon (SOC) sequestration. However, quantifying SOC stocks and monitoring carbon (C) fluxes in rangelands are challenging due to the considerable spatial and temporal variability tied to rangeland C dynamics as well as limited data availability. We developed the Rangeland Carbon Tracking and Management (RCTM) system to track long-term changes in SOC and ecosystem C fluxes by leveraging remote sensing inputs and environmental variable data sets with algorithms representing terrestrial C-cycle processes. Bayesian calibration was conducted using quality-controlled C flux data sets obtained from 61 Ameriflux and NEON flux tower sites from Western and Midwestern US rangelands to parameterize the model according to dominant vegetation classes (perennial and/or annual grass, grass-shrub mixture, and grass-tree mixture). The resulting RCTM system produced higher model accuracy for estimating annual cumulative gross primary productivity (GPP) ($R^2 > 0.6$, RMSE $< 390 \text{ g C m}^{-2}$) relative to net ecosystem exchange of CO_2 (NEE) ($R^2 > 0.4$, RMSE $< 180 \text{ g C m}^{-2}$). Model performance in estimating rangeland C fluxes varied by season and vegetation type. The RCTM captured the spatial variability of SOC stocks with $R^2 = 0.6$ when validated against SOC measurements across 13 NEON sites. Model simulations indicated slightly enhanced SOC stocks for the flux tower sites during the past decade, which is mainly driven by an increase in precipitation. Future efforts to refine the RCTM system will benefit from long-term network-based monitoring of vegetation biomass, C fluxes, and SOC stocks.

© 2025 The Author(s). Journal of Advances in Modeling Earth Systems published by Wiley Periodicals LLC on behalf of American Geophysical Union. This is an open access article under the terms of the [Creative Commons Attribution License](https://creativecommons.org/licenses/by/4.0/), which permits use, distribution and reproduction in any medium, provided the original work is properly cited.

Zhongming Gao, Jiquan Chen,
Michael Abraha, Russell L. Scott, Gerald
N. Flerchinger, Patrick E. Clark, Paul
C. Stoy, Anam M. Khan,
E. N. Jack Brookshire, Quan Zhang, David
R. Cook, Thomas Thienelt, Bhaskar Mitra,
Marguerite Mauritz-Tozer, Craig
E. Tweedie, Margaret S. Torn,
Dave Billesbach

Formal analysis: Yushu Xia, Megan
B. Machmuller, Andrew L. Mullen,
Charlotte Rivard, Arthur Endsley,
Haydee Hernandez

Funding acquisition: Yushu Xia,
Jonathan Sanderman, Jennifer D. Watts,
Megan B. Machmuller, Stephanie
A. Ewing

Investigation: Yushu Xia,
Jonathan Sanderman, Jennifer D. Watts,
Megan B. Machmuller, Andrew L. Mullen,
Charlotte Rivard, Arthur Endsley,
Haydee Hernandez

Methodology: Yushu Xia,
Jonathan Sanderman, Jennifer D. Watts,
Megan B. Machmuller, Andrew L. Mullen,
Charlotte Rivard, Arthur Endsley,
Haydee Hernandez

Project administration:
Jonathan Sanderman, Jennifer D. Watts,
Megan B. Machmuller

Resources: Yushu Xia,
Jonathan Sanderman, Jennifer D. Watts,
Megan B. Machmuller, John Kimball,
Stephanie A. Ewing, Marcy Litvak,
Tomer Duman, Praveena Krishnan,
Tilden Meyers, Nathaniel A. Brunsell,
Binayak Mohanty, Heping Liu,
Zhongming Gao, Jiquan Chen,
Michael Abraha, Russell L. Scott, Gerald
N. Flerchinger, Patrick E. Clark, Paul
C. Stoy, Anam M. Khan,
E. N. Jack Brookshire, Quan Zhang, David
R. Cook, Thomas Thienelt, Bhaskar Mitra,
Marguerite Mauritz-Tozer, Craig
E. Tweedie, Margaret S. Torn,
Dave Billesbach

Software: Yushu Xia, Andrew L. Mullen,
Charlotte Rivard, Arthur Endsley,
Haydee Hernandez

Supervision: Jonathan Sanderman,
Jennifer D. Watts, John Kimball, Stephanie
A. Ewing

Validation: Yushu Xia, Andrew
L. Mullen, Charlotte Rivard,
Arthur Endsley

Visualization: Yushu Xia,
Jonathan Sanderman

Writing – original draft: Yushu Xia

Writing – review & editing: Yushu Xia,
Jonathan Sanderman, Jennifer D. Watts,
Megan B. Machmuller, Andrew L. Mullen,
Charlotte Rivard, Arthur Endsley,
Haydee Hernandez, John Kimball,
Marcy Litvak, Tomer Duman,
Praveena Krishnan, Tilden Meyers,
Nathaniel A. Brunsell, Binayak Mohanty,
Heping Liu, Zhongming Gao,
Jiquan Chen, Michael Abraha, Russell
L. Scott, Gerald N. Flerchinger, Patrick
E. Clark, Paul C. Stoy, Anam M. Khan,
E. N. Jack Brookshire, Quan Zhang, David

Plain Language Summary Rangelands play a crucial role in providing various ecosystem services, including potential climate change mitigation through increased soil organic carbon (SOC) storage. Accurate estimates of changes in carbon (C) storage are challenging due to the heterogeneous nature of rangelands and the limited availability of field observations. In this work, we leveraged remote sensing observations, tower-based C flux measurements from over 60 rangeland sites in the Western and Midwestern US, and other environmental data sets to build the process-based Rangeland Carbon Tracking and Management (RCTM) modeling system. The RCTM system is designed to simulate the past 20 years of rangeland C dynamics and is regionally calibrated. The RCTM system performs well in estimating spatial and temporal rangeland C fluxes as well as spatial SOC storage. Model simulation results revealed increased SOC storage and rangeland productivity driven by annual precipitation patterns. The RCTM system developed by this work can be used to generate accurate spatial and temporal estimates of SOC storage and C fluxes at fine spatial (30 m) and temporal (every 5 days) resolutions, and is well-suited for informing rangeland C management strategies and improving broad-scale policy making.

1. Introduction

Rangelands, which include a wide range of semi-arid to arid landscapes primarily composed of grasses, forbs, and shrubs that are often grazed or browsed by domestic livestock and/or wildlife. Rangelands cover more than 30% of the land area (~2.7 million km²) of the contiguous United States and 54% of all land globally (Chen et al., 2015; Olson et al., 2001; Reeves & Mitchell, 2011). These landscapes provide many crucial ecosystem services, including habitat biodiversity, forage production, water retention, nutrient cycling, and climate regulation (Maher et al., 2021; Phukubye et al., 2022; Waterhouse et al., 2023). Unfortunately, grassland conversion to cropland and improper management (e.g., overgrazing) have historically contributed to land degradation and C loss in western US rangelands, which can be further exacerbated by extreme climate events such as droughts (Holechek et al., 2020). Restoring degraded rangelands through improved land management is a high priority conservation goal with multiple ecosystem service benefits (Wilson et al., 2008). Improved rangeland management also holds possibly significant but highly uncertain potential for climate change mitigation primarily through soil organic carbon (SOC) sequestration (Derner et al., 2019; Fargione et al., 2018). The uncertainty arises from multiple factors, including limited availability of in-situ field data and substantial spatial and temporal variability associated with environmental and management drivers of SOC change, such as moisture status and temperature, vegetation composition, soil properties, and grazing timing and intensity (Booker et al., 2013; Derner & Schuman, 2007; Hill et al., 2006).

In-situ field measurements, when available, provide crucial observations of rangeland C dynamics. Flux tower observations are often used to quantify net ecosystem exchange (NEE), which represents C fluxes between land and atmosphere that can be further partitioned into gross primary productivity (GPP) and ecosystem respiration (RECO) (Oliphant, 2012; Tramontana et al., 2020). Field sampling campaigns are essential for directly measuring SOC stocks and investigating the associated spatial heterogeneity and temporal changes (Nave et al., 2021), which complements C fluxes observed from flux towers. However, direct field measurements can be expensive and labor-intensive, often requiring many sampling locations to accurately represent variations in ecosystem properties within vast and complex rangeland regions. Upscaling in-situ observations of C fluxes and SOC stocks using models coupled with remote sensing (RS) and large-scale, surveys-derived environmental variable data sets can help overcome limitations inherent from using field data alone, allowing for the spatially explicit tracking of GPP, RECO, NEE and SOC change and longer-term C budgets across large geographic scales (Heuvelink et al., 2021; Krause et al., 2022; Sanderman et al., 2017; Turner et al., 2004).

Another approach to upscaling field data is through process-based modeling of C fluxes and SOC stocks, which can be implemented using two strategies, namely a management-driven approach or an RS-driven approach. In the management-driven approach, activity data such as livestock numbers and grazing periods are combined with climate and soil information to simulate plant growth and soil C dynamics (Arndt et al., 2022; Smith et al., 2014; W. Zhang et al., 2017). Adopting this approach necessitates the collection of detailed management data, which can be fairly difficult for large-scale rangeland monitoring efforts. Even though there has been a major push to automate the collection of management data through the use of RS, tracking animal numbers and movements

R. Cook, Thomas Thienelt, Bhaskar Mitra,
Marguerite Mauritz-Tozer

remains challenging (Ali et al., 2016; Lange et al., 2022; Stoy et al., 2021). To estimate management effects on SOC, current rangeland modeling efforts typically rely on the use of default parameters and model structures, such as those used in DAYCENT (Chang et al., 2015; Parton et al., 1998), Denitrification-Decomposition (DNDC) (C. Li et al., 1994; G. Wang et al., 2022), and Rothamsted Carbon (RothC) (Coleman & Jenkinson, 1996; Jebari et al., 2021) because there is a general lack of calibration and validation data suited to represent specific management scenarios (e.g., adaptive grazing practices). Due to such data limitations, the management-driven process-based modeling approach may sometimes struggle to account for system variability and generate predictions at the scale that is relevant to management.

The use of RS data to drive process-based modeling is particularly helpful in situations where management data sets are unavailable or scarce, because RS data can provide information needed to track vegetation productivity, growth, and disturbances (e.g., drought and grazing) due to the close association between plant characteristics and RS spectral bands or multi-band indices (Feldman et al., 2024; Numata et al., 2007; Sibanda et al., 2016; Xu et al., 2008). Moreover, RS data sets can provide more refined information regarding ecosystem dynamics and spatiotemporal variability, which would be difficult to capture using management data sets alone. Utilizing RS for rangeland monitoring assumes that RS can adequately capture management effects via changes in plant cover and productivity. Because this assumption is largely untested in rangeland settings, ground-truth data is crucial for the parameterization and evaluation of RS-driven models for rangeland monitoring (Reinermann et al., 2020). Large data sets collected through network-based measurements, such as flux tower-based observations of C fluxes and field-based measurements of SOC stocks (Biederman et al., 2017; Chu et al., 2023; Hinckley et al., 2016), offer the best representation of rangeland C dynamics under different soil, climate, and vegetation conditions, and thus are well-suited for regional model calibration and validation.

The RS-driven modeling approach has a long legacy for use in cropping, wetland, and forest systems (J. Wang et al., 2011; Watts et al., 2023; Zhou et al., 2021) and global scale monitoring (Endsley et al., 2020); however, to the best of our knowledge, there has not been an RS-driven regional model designed and parameterized specifically for US rangelands to evaluate C dynamics and SOC changes at high spatial resolutions, sub-weekly timesteps, for different vegetation groups, and across decadal-scale periods. Therefore, our research objectives were twofold. First, we developed a new framework, namely the Rangeland Carbon Tracking and Management (RCTM) system, which: (a) incorporates fine-resolution, long-term geospatial data sets that can be obtained either from publicly available sources or through data fusion, as model inputs, (b) derives regional vegetation class-specific parameters through model calibration and validation using flux tower network-based C flux data sets (i.e., GPP and NEE) collected from Western and Midwestern US rangelands, and (c) simulates rangeland C dynamics and SOC changes in the past 20 years for case study sites while identifying the main driving factors. The second objective was to evaluate the model by estimating vegetation type-specific annual and seasonal cumulative and daily GPP and NEE, as well as spatial SOC stocks, with the goal of determining whether the regionally-calibrated RCTM system can achieve sufficient accuracy for spatiotemporal estimates of rangeland C fluxes and identifying areas and vegetation groups where model improvements are necessary. The RCTM system is designed not only to provide spatially detailed (30 m) estimates and visualizations of rangeland C dynamics from 2003 to the present, but also to identify key environmental drivers, remaining uncertainties, and knowledge gaps in current C modeling efforts, which are anticipated to support land managers and policymakers with actionable insights for improved rangeland monitoring and management.

2. Materials and Methods

2.1. Overview of the Rangeland Carbon Tracking and Management (RCTM) System

To provide a framework tracking regional rangeland C dynamics, we developed RCTM as a process-based RS-driven modeling system. The system integrates RS-informed geospatial data sets and in-situ field measurements with process-based representation of the C cycle (Table S1 in Supporting Information S1). The RCTM system first estimates plant productivity using RS and environmental inputs. The estimates are then fed into a process-based ecosystem model to simulate C dynamics. There are four main components involved in the system (Figure 1): fraction of absorbed photosynthetically active radiation (fPAR) calculation; GPP (CO₂ uptake) calculation; biomass and C pool estimates; C flux and SOC stock estimates.

First, the Spatial and Temporal Adaptive Reflectance Fusion Model (STARFM) algorithm (F. Gao et al., 2006; Watts et al., 2011) is utilized to derive estimates of the fPAR at a 30 m resolution and at 5-day intervals. This is

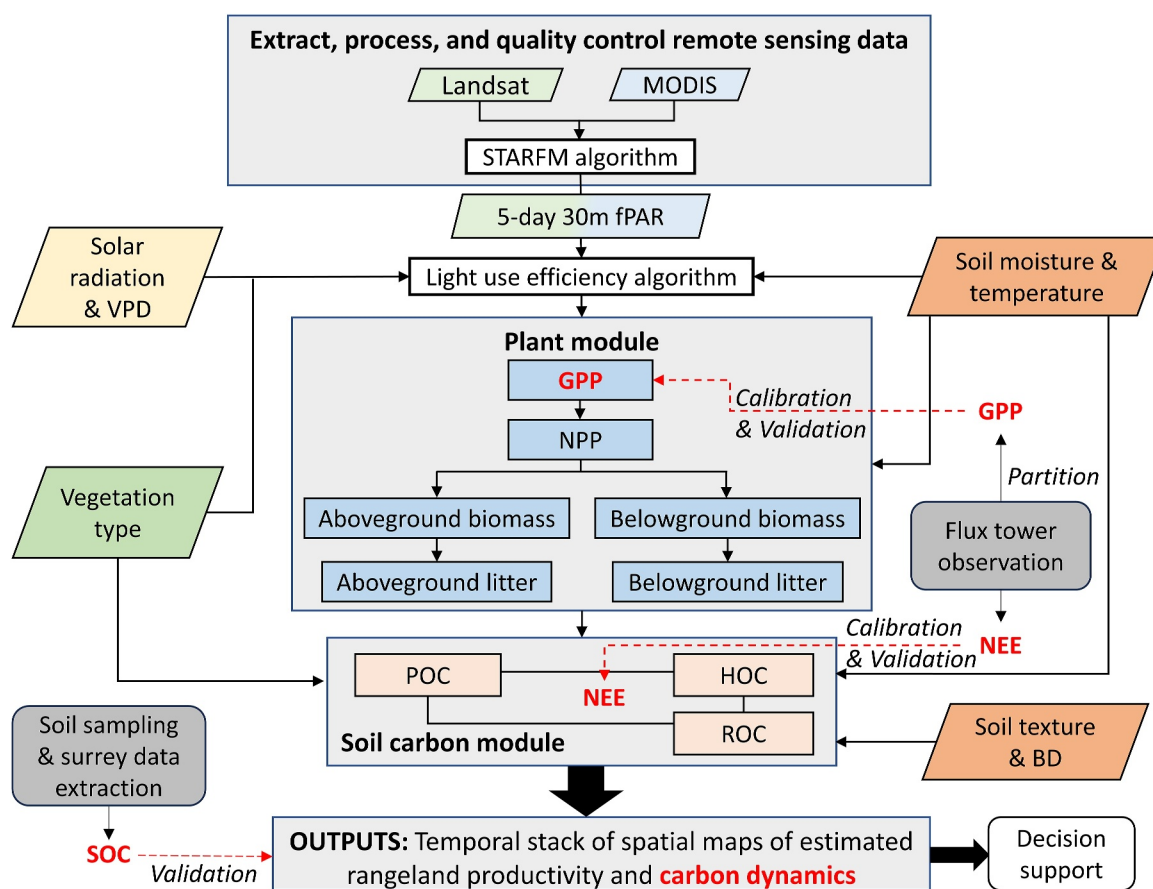


Figure 1. Components of Rangeland Carbon Tracking and Management (RCTM) system. The primary RCTM inputs include remote sensing (RS) images, soil properties (soil texture, bulk density (BD), soil moisture, and soil temperature), climate data (vapor pressure deficit (VPD) and solar radiation), and vegetation type. The outputs include spatial and temporal estimates of rangeland productivity and carbon dynamics. RS images are fused using the Spatial and Temporal Adaptive Reflectance Fusion Model (STARFM) algorithm to obtain records of normalized difference vegetation indices (NDVI); NDVI is then used within a ratio approach to derive the fraction of absorbed photosynthetically active radiation (fPAR) values. The model is calibrated and validated against gross primary productivity (GPP, $\text{g C m}^{-2} \text{d}^{-1}$), net ecosystem exchange (NEE, $\text{g C m}^{-2} \text{d}^{-1}$) of CO_2 , and soil organic carbon (SOC). The plant module estimates net primary productivity (NPP) and aboveground and belowground biomass and litter; the soil carbon module includes particulate organic carbon (POC), humus organic carbon (HOC), and resistant organic carbon (ROC) pools.

accomplished using a normalized difference vegetation index (NDVI) ratio approach (Section 2.4; described in Peng et al. (2012); Watts et al. (2024)). Second, RS or survey-derived variables, including soil properties, climate factors, and vegetation types, are utilized in conjunction with fPAR through light-use efficiency (LUE) algorithms adapted from NASA's Soil Moisture Active-Passive (SMAP) Level 4 Carbon (L4C) model (Endsley et al., 2020) to derive estimates of GPP, where vegetation type-specific parameters associated with environmental variable-based constraints on LUE are subject to model calibration (Figure S1 in Supporting Information S1). The third component (Figure S2 in Supporting Information S1) estimates aboveground and belowground biomass from GPP using algorithms adapted from DAYCENT (Parton et al., 1998). Model simulated biomass C inputs are then allocated to different SOC pools within a process-based model structure adapted from the RothC model (Coleman & Jenkinson, 1996). The SOC pools include particulate organic C (POC), humus organic C (HOC), and resistant organic C (ROC) pools that are associated with fast, intermediate, and slow SOC turnover rates, respectively. In the fourth step, RCTM derives estimates of C fluxes and SOC stocks, with flux tower-based measurements of NEE used to parameterize factors controlling C flows among different biomass and SOC pools (Figure S2 in Supporting Information S1).

Aside from RS-derived NDVI records, the main inputs for RCTM include soil properties (soil texture, moisture, and temperature), climate variables (air temperature, vapor pressure deficit (VPD), solar radiation), and vegetation cover type represented by fractional coverage of different vegetation types (Table 1). Although some

Table 1
Input Environmental Data sets for the Rangeland Carbon Tracking and Management (RCTM) System

Data type	Variables ^a	Original resolution		Full temporal coverage	Usage ^b	Source and reference ^c
		Spatial	Temporal			
Soil properties	Clay%	100 m	Only once in time		Model spin-up, NEE calibration, SOC estimation, and site-based correlation analysis	SoilGrids+ (Rancharan et al., 2018)
	Surface and root zone soil moisture	0.125°	Hourly	Since 1979	GPP calibration, model spin-up, NEE calibration, SOC estimation, and site-based correlation analysis	NLDAS (Xia et al., 2012)
	Surface soil temperature				GPP calibration, model spin-up, NEE calibration, SOC estimation, and site-based correlation analysis	
Climate	VPD	1 km	Daily	Since 1980	GPP calibration and site-based correlation analysis	DAYMET v4 (Thornton et al., 2022)
	Air temperature	1 km	Daily	Since 1980	Site-based correlation analysis	
	Precipitation					
Biotic	Solar Radiation	0.125°	Hourly	Since 1979	GPP calibration	NLDAS (Xia et al., 2015)
	fPAR	500 m	Every 4 days	Since 2002	GPP calibration (coarse resolution) shown in Text S1 in Supporting Information S1	MODIS (Schaaf & Wang, 2015)
Topography	Land cover type%	30 m	Every 5 days	Since 2002	GPP calibration (fine resolution) and site-based correlation analysis	STARFM (F. Gao et al., 2006; Watts et al., 2011)
	Elevation	30 m	Annually	Since 1984	Vegetation type assignment	RAP (Jones et al., 2018)
	Slope	30 m	Only once in time		Site-based correlation analysis	SRTM (van Zyl, 2001)

^aClay%: soil clay content; fPAR: fraction of absorbed photosynthetically active radiation; VPD: vapor pressure deficit. ^bGPP, gross primary productivity; NEE, net ecosystem exchange of CO₂; SOC, soil organic carbon. ^cDAYMET, Daily Surface Weather and Climatological Summaries; MODIS, Moderate Resolution Imaging Spectroradiometer; NLDAS, North American Land Data Assimilation System; RAP, Rangeland Analysis Platform; SRTM, Shuttle Radar Topography Mission.

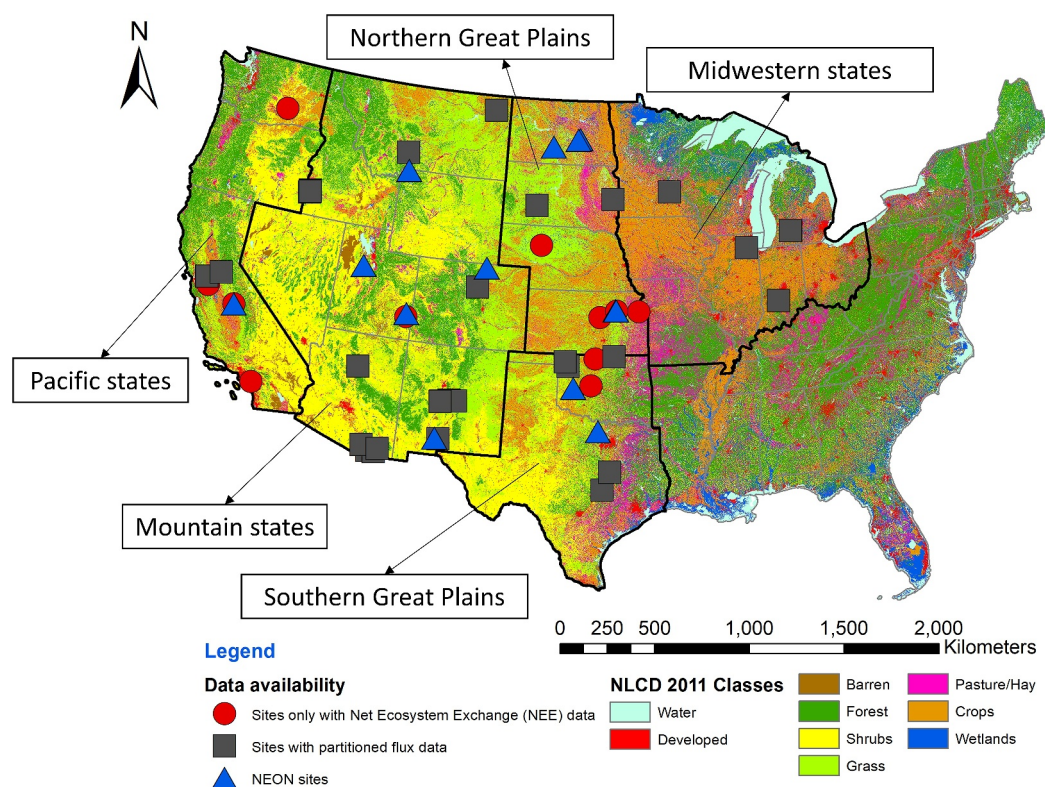


Figure 2. Ameriflux and National Ecological Observatory Network (NEON) sites selected for model calibration and validation. The sites are divided into different groups based on data availability. Different U.S. Department of Agriculture (USDA) agricultural regions are delineated by thick black lines, and different land use types are color-coded according to the National Land Cover Database (NLCD) data set.

environmental factors are used in both the GPP and NEE modules of RCTM (Figure 1), their thresholds are parameterized separately for each modeling component. Model outputs include 30 m resolution estimates of rangeland productivity represented by GPP at 5-day intervals, net C fluxes represented by NEE at 5-day intervals, and annual SOC stocks over the 20-year record (2003–2022). The development and application steps for RCTM are outlined in Figure S3 in Supporting Information S1.

2.2. Study Sites and Data Sources

For model parameterization, study sites were selected from the Ameriflux (Novick et al., 2018; <https://ameriflux.lbl.gov/>) and National Ecological Observatory Network (NEON) networks (Keller et al., 2008; <https://www.neonscience.org/>) within the Western and Midwestern US states (Figure 2). We first identified all of the flux tower sites located within the region and classified as grasslands (“GRA”), savannas (“SAV”), or open shrublands (“OSH”) by Ameriflux or NEON. These sites were supplemented with those identified under grassland or pasture-relevant classes according to the National Land Cover Database (NLCD) data layers (Homer et al., 2007, 2015). We then screened the identified sites to include only those dominated by grass coverage by surveying publications associated with the flux tower data sets, examining Phenocam images (Brown et al., 2016) or online photos, and reaching out to tower principal investigators (PIs) for confirmation. Ideally, perennial and annual grasses would be separated into two categories, but this is currently not feasible due to the limited number of sites with annual grasses in the retained data set. The classification was determined using land cover information extracted from the NLCD and Rangeland Analysis Platform (RAP) (Jones et al., 2018), published information, and PI-provided site data. For this study, we defined class (1) as native grasslands or grasslands without explicit descriptions of active management practices. Sites included in the managed hay and pasture class differ from class (1) because these sites are being actively managed, meaning that there is some combination of sown grass species, irrigation, and fertilization. However, the number of hay and pasture sites is relatively small, and some sites in the perennial and/or annual grass class may actually belong in the hay and pasture class but are misclassified due to a

lack of management data. Therefore, class (2) consists of hay and pasture sites and is used solely for model validation in this study. The coverage threshold for shrubs and trees was set at 30% for classes (3) and (4), meaning grass-shrub mixture and grass-tree mixture, respectively. Additional details regarding the Ameriflux and NEON sites can be found in Table S2 in Supporting Information S1.

We acquired flux observations and environmental variable data sets for the retained Ameriflux and NEON sites, either from the online portal (<https://ameriflux.lbl.gov/>) or directly from flux tower PIs. We also documented site location, soil and vegetation type, flux tower height, data coverage, and variable availability for each site (Table S2 in Supporting Information S1). Based on data availability, the sites were further divided into three categories (Figure 2). The first group includes sites reporting NEE measurements only; the second group includes those that provide both NEE and model-partitioned GPP and RECO data; and the third group consists of sites belonging to the NEON network, which have SOC measurements in addition to NEE, GPP, and RECO data (Hinckley et al., 2016). In some cases, tower PIs expressed concerns about the quality of GPP data due to flux partitioning issues (Desai et al., 2008; Sulman et al., 2016). Consequently, we assigned these sites to the first category. Overall, we obtained data from 17, 31, and 13 sites in categories 1, 2, and 3, respectively. The flux data sets from the retained sites were quality-controlled and harmonized using standard methods (Section 2.3) before being used for model calibration and validation (Sections 2.5 and 2.6).

To represent the approximate footprint of the flux towers, shapefiles were created in R (R Core Team, 2023), using small (90 m × 90 m) or large (510 m × 510 m) grid sizes, which were determined based on a threshold value of 8 m, corresponding to the flux tower height (Table S2 in Supporting Information S1). The shapefiles were used for extraction of MODIS and Landsat RS inputs, as well as variable inputs in subsequent steps (Figure 1).

2.3. Quality Control of C Flux Data Sets

Several quality control (QC) measures were applied to the C flux (NEE and GPP) data sets to alleviate bias that can influence subsequent model parameterization steps. First, daily GPP and NEE results, as well as the associated meteorological measurements (e.g., air temperature, precipitation), were aggregated from the original half-hourly time step and then plotted to allow the visual identification of potential outliers or noise including: (a) extended periods with GPP reported as zero, especially during the growing season; (b) multiple GPP peaks with similar magnitudes observed during the growing season; (c) irregular spikes or sudden changes in GPP or NEE, particularly during the non-growing season. For sites with observations falling within category (1), we worked with flux tower PIs to determine whether it was necessary to replace the identified data points with no-value (NaN) flags. In the case of data points identified by category (2), we consulted with flux tower PIs to confirm whether the presence of multiple peaks could be attributed to grazing or the growth of multiple vegetation species (e.g., C3 and C4) at the sites before determining whether to retain the data points. Finally, outlier peaks identified in category (3) were removed using a moving window approach adapted from the outlier removal methods designed for time series data sets (Hartigan et al., 2019; Kelley, 2013). This involved establishing the median value of a 15-day period as a reference value, and then any observation that deviated from its reference by more than twice the standard deviation of the flux measurements at the site level was removed. The quality-controlled daily GPP and NEE data sets were then classified into the four vegetation types defined in Section 2.2.

2.4. RS Data Extraction and Processing

We derived 30 m estimates of NDVI at 5-day intervals by employing the STARFM algorithm (F. Gao et al., 2006; Watts et al., 2011), which leverages the high temporal resolution of MODIS inputs (500 m, daily) and high spatial resolution of Landsat (30 m, every 8 days). We first obtained MODIS imagery from the Nadir Bidirectional Reflectance Distribution Function Adjusted Reflectance (NBAR) product (MCD43A4 V6) (Schaaf & Wang, 2015) for each study site. Data was quality filtered using standard QC measures. These included the removal of cloudy pixels using the product cloud bitmask and an additional filtering to exclude snow-covered pixels, based on the normalized difference snow index (Hall et al., 2002). Subsequently, we calculated temporal averages at the pixel level over a 20-day moving window as a smoothed data set, which was used to replace missing data or cropped pixels from the previous step. Landsat imagery was combined from Landsat 5, 7, and 8 surface reflectance products from Collection 2 (Kovalsky & Roy, 2013; Roy et al., 2014; Williams et al., 2006) to derive long-term records with finer 8-day temporal fidelity than the standard 16-day repeat sampling from individual Landsat satellites. QC was carried out to first exclude cloudy and snow-covered pixels using the dilated

cloud, cirrus, cloud shadow, and snow bitmasks. After applying the dilated cloud bitmask, haze, and thin cloud edges were often still present based on visual assessment of Landsat imagery. These cloud remnants were removed by applying an additional 15-pixel radius buffer. Images containing considerable cloud and snow contamination (>60%) were removed from the time series. To account for Landsat 7 scan-line gaps and to recover image areas that were removed from the augmented cloud masking, the masked Landsat images were spatially gap-filled using local histogram matching (United States Geological Survey, 2019). First, a median composite image was generated with the nearest 2 months of imagery. Then, a linear regression was used to determine the line of best fit between pixels in the composite image and pixels in the cloud-masked image within a 50-pixel moving window. Linear regression coefficients within each moving window were applied to the composite image to fill “no data” pixels in the masked image. Finally, pixels containing water were removed using the water bitmask.

The resulting QC/processed MODIS and Landsat scenes that overlapped on the same dates were input into the STARFM algorithm (F. Gao et al., 2006; Watts et al., 2011). STARFM uses comparisons of the Landsat/MODIS image pairs to predict spectral maps at a 30 m spatial resolution across the input MODIS image time series. The resulting fused red and near-infrared bands were used to derive estimates of NDVI (Tucker, 1979) and scaled surface reflectance (SSR; Equation 2). Erroneous NDVI observations were filtered by removing values where the rolling 14-day median was greater than two times the rolling 365-day standard deviation. This conservative filter mainly functioned to remove NDVI observations over snow and clouds that were missed during masking. Temporal gaps in NDVI were filled using linear interpolation.

$$SSR = \frac{1 + NDVI}{1 - NDVI} \quad (1)$$

Finally, fPAR was calculated using Equations 2–4, with the minimum and maximum NDVI and SSR reference thresholds corresponding to the 2nd and 98th percentiles of the time series values for all retained Ameriflux sites. The minimum and maximum fPAR reference values were determined through Monte-Carlo analysis for each vegetation type. The predicted GPP was compared with the observed GPP (see Section 2.5), and the optimal combination of values that resulted in the best-fitted vegetation type-specific model were determined as fPAR reference values.

$$fPAR_{NDVI} = \frac{(NDVI - NDVI_{min}) \times (fPAR_{max} - fPAR_{min})}{(NDVI_{max} - NDVI_{min})} \quad (2)$$

$$fPAR_{SSR} = \frac{(SSR - SSR_{min}) \times (fPAR_{max} - fPAR_{min})}{(SSR_{max} - SSR_{min})} \quad (3)$$

$$fPAR = \frac{fPAR_{NDVI} + fPAR_{SSR}}{2} \quad (4)$$

The extraction and QC processing of both MODIS and Landsat data were implemented within the Google Earth Engine (GEE) platform (Gorelick et al., 2017), while the implementation of the STARFM algorithm and the following RS data processing steps were realized using Python (Rossum & Drake, 1995). All the codes used in this and subsequent sections are openly available via Zenodo: <https://zenodo.org/records/11508223>.

2.5. GPP Model Estimation and Calibration

The LUE algorithms used for the GPP calculation were adapted from the SMAP's L4C model (Endsley et al., 2020). In RCTM, the estimation of actual LUE is based on scaling the potential maximum LUE by modifiers including root zone (ca. 60 cm depth) soil moisture (S_{mult}), surface 5 cm soil temperature (T_{mult}), and VPD (W_{mult}) (Figure S1 in Supporting Information S1 and Equation 5), where threshold values (i.e., maximum and minimum) for these modifiers were established for both upper and lower bound values. The daily GPP is calculated based on estimated LUE, STARFM-derived fPAR detailed in Section 2.4, and shortwave incoming solar radiation (SW_IN) using Equation 6.

$$LUE = LUE_{max} \times S_{mult} \times T_{mult} \times W_{mult} \quad (5)$$

$$\text{GPP} = \text{LUE} \times \text{SW_IN} \times 0.45 \times \text{fPAR} \quad (6)$$

where GPP represents daily gross primary productivity (g C m^{-2}), LUE represents light use efficiency (g C MJ^{-1}) estimated based on maximum LUE adjusted by environmental modifiers, SW_IN represents shortwave incoming solar radiation (MJ m^{-2}), fPAR represents fraction of absorbed photosynthetically active radiation, and 0.45 indicates the standard assumption that about 45% of incoming shortwave radiation is photosynthetically active (He et al., 2022).

To facilitate GPP calibration, we extracted root zone soil moisture, soil temperature at 5 cm surface depth, SW_IN from NLDAS (Xia et al., 2012), and VPD from Daymet V4 (Thornton et al., 2022) for the Ameriflux and NEON sites. We used GEE for the direct extraction of NLDAS-derived SW_IN and Daymet-derived VPD at a daily time step. Soil moisture and temperature were downloaded from the NASA Earthdata portal using the subset tools, then averaged to daily values in Google Collaboratory and stored in Google Cloud (Google Inc., CA, USA). The extracted environmental variable data sets were merged with STARFM fPAR every 5 days. Next, the merged data set was joined with GPP measurements processed from Section 2.3. The resulting final calibration data set contained GPP records (302 site-year combinations) from 47 sites (Table S3 in Supporting Information S1).

We carried out model calibration by adjusting vegetation type-based threshold values associated with the environmental modifiers, including minimum and maximum values of root zone soil moisture (%), soil temperature ($^{\circ}\text{C}$), and VPD (Pa), as well as maximum LUE (Figure S1 in Supporting Information S1), using GPP fluxes from all 47 sites (Figure 1). In this approach, a single set of vegetation type-specific model parameters was derived, rather than separate parameter sets for individual sites. The calibration followed an iterative Bayesian calibration approach, with initial values and bounds informed by SMAP's L4C model (Endsley et al., 2020; for grass, tree, and shrub classes), further informed by relevant literature, and empirical estimations. These parameters were then refined through model calibration runs, allowing for progressive updates based on the results of each iteration. The procedure was implemented using the BayesianTools package in R (Hartig et al., 2023) with the Differential-Evolution sampling algorithm (Ter Braak & Vrugt, 2008). Three Markov Chain Monte Carlo (MCMC) chains were run in parallel for 10,000 iterations to obtain posterior distributions of model parameters, assuming weakly informative priors. Model convergence was examined using the scale reduction factor (Gelman & Rubin, 1989), and the resulting model parameter distributions are presented in Table S4 and Figures S3–S5 in Supporting Information S1.

The vegetation type-based model fits were reported along with results from leave-one-out cross-validation (LOOCV) for daily and cumulative (monthly, seasonal, and annual) GPP models. The LOOCV approach involved iteratively excluding one site at a time from the data set, recalibrating the model using the remaining sites, and validating against the excluded site. This method avoids issues that arise when randomly selected validation sites fail to represent overall model performance. Error metrics including Coefficient of Determination (R^2 ; Equation 7), Root Mean Square Error (RMSE; Equation 8), Mean Bias Error (MBE; Equation 9), normalized RMSE (nRMSE; Equation 10), and Relative Bias (RB; Equation 11), were calculated for perennial and/or annual grass, grass-shrub mixture, and grass-tree mixture classes. For the managed hay and pasture class, model validation was conducted using perennial and/or annual grass-specific parameters, due to the limited number of available training sites. The model calibration procedure was also carried out using MODIS fPAR inputs to enable a comparison with the use of STARFM inputs, which is detailed in Text S1 in Supporting Information S1. Additional evaluations of GPP models, along with detailed model comparison between the use of MODIS and STARFM inputs, are presented in Figures S6, S7, Tables S5, and S6 in Supporting Information S1.

$$R^2 = 1 - \frac{\sum_{i=1}^n (y_i - \hat{y}_i)^2}{\sum_{i=1}^n (y_i - \bar{y})^2} \quad (7)$$

$$\text{RMSE} = \sqrt{\frac{\sum_{i=1}^n (y_i - \hat{y}_i)^2}{n}} \quad (8)$$

$$\text{MBE} = \frac{\sum_{i=1}^n (\hat{y}_i - y_i)}{n} \quad (9)$$

$$nRMSE = \frac{RMSE}{\bar{y}} \quad (10)$$

$$RB = \frac{MBE}{\bar{y}} \quad (11)$$

where n represents the number of samples, y_i represents observed value of sample i , \hat{y}_i represents the model predicted value of sample i , and \bar{y} represents the mean of observations.

2.6. Carbon Model Spin-Up, Calibration, and Validation

The RCTM model adopts SMAP's L4C scheme (Endsley et al., 2020) by allocating GPP into net primary productivity (NPP) and autotrophic respiration. The NPP was further partitioned into aboveground and belowground biomass using root to shoot ratio specific to the three vegetation types. While more detailed parameterization for partitioning aboveground and belowground biomass is desirable, it has not been implemented in the current version of RCTM to preserve model parsimony. To account for the formation of litter (e.g., dead plant material) over time, we adopted DAYCENT's algorithms (Parton et al., 1998). These algorithms compute the C transfer from biomass pools into surface litter and dead roots at each time step, influenced by factors such as the day of the year, soil moisture, and soil temperature. Subsequently, RCTM simulates C transfer from aboveground and belowground litter pools to SOC pools. The SOC module of RCTM was adapted from the RothC model structure (Coleman & Jenkinson, 1996), which includes three measurable soil C pools equivalent to fast (i.e., POC), intermediate (i.e., HOC), and slow (i.e., ROC) pools. The dynamics of C flow among these SOC pools are controlled by factors including soil texture, soil moisture, and soil temperature (Figure S2 in Supporting Information S1).

In RCTM, biomass and soil C pools were initialized by running the model for 2,000 years to reach an equilibrium that ensures the soil system is in equilibrium with the environmental conditions being simulated. The inputs for the spin-up were set to represent a "typical" condition with a seasonal cycle for each site, for which we utilized STARFM fPAR, both surface 5 cm and root depth (ca. 60 cm) soil moisture, 5 cm soil temperature, and clay content averaged from the 2002–2005 period. Soil moisture and temperature data were extracted from the NLDAS database (Xia et al., 2012), and clay content were obtained from the SoilGrids + product (Ramcharan et al., 2018) (Table 1). Before conducting NEE calibration, we performed model spin-up for all retained Ameriflux and NEON sites using default model parameters obtained from SMAP's L4C, DAYCENT, and RothC models (Table S1 in Supporting Information S1). GPP estimates, which are required for SOC calculation, were simulated using vegetation type-specific calibrated GPP parameters and inputs specified in Section 2.5. Both GPP and environmental variable data sets needed for model initialization were aggregated to a 5-day time step by averaging the results across all years. The goal was to obtain site-specific estimates of initial C pools to expedite the subsequent NEE calibration process.

The next step involved matching the input variable data sets needed for NEE calibration with NEE flux observations. The model input data was processed from its original resolution to a 5-day interval to align with the resolution of the STARFM outputs. The combined data set includes 22,820 NEE observations (364 site-year combinations) from 59 sites (Table S3 in Supporting Information S1). We then carried out model calibration by optimizing vegetation type-specific parameters related to biomass partitioning, litterfall, and SOC decomposition (Figure S2 in Supporting Information S1) using NEE observations (Figure 1). In the calibration process, site-based estimates of initial C pools were used to spin up the model and then calculate C fluxes for 2002–2022. The calibration was implemented following the same MCMC procedure used for the GPP model (See Section 2.5), except that 5,000 iterations were used to obtain posterior distributions by considering the computational time and cost. Again, model calibration was also implemented using MODIS-based fPAR inputs to enable a comparison with the use of STARFM inputs, which is presented in Figure S8 and Table S6 in Supporting Information S1, and explained by Text S1 in Supporting Information S1. Model performance for estimating RECO is provided in Figure S9 and Table S7 in Supporting Information S1, where the absolute values of RECO fluxes were calculated as the difference between GPP and NEE.

After obtaining vegetation type-specific parameters through GPP and NEE calibrations, we ran RCTM for NEON sites to derive estimates of surface depth SOC stocks. Because the depth represented by RCTM cannot be clearly

defined considering the depths represented by model input layers, the results were compared against measurements of both 0–30 cm and 0–100 cm SOC stocks from 13 NEON sites (Figure S10 in Supporting Information S1) as an evaluation of model performance for ranking the amount of SOC stocks in space.

2.7. Estimates of Carbon Fluxes for Flux Tower Sites

The calibrated RCTM model was applied to all retained Ameriflux and NEON sites to derive estimates of GPP, NEE, and SOC stocks for a 20-year period (2003–2022). After averaging model outputs to annual results, the Pearson correlation coefficients were calculated in R between model input variables and RCTM outputs for site-year combinations. The purpose of this analysis was to explore potential climate and soil controls on the spatiotemporal dynamics in model-simulated C fluxes. We aggregated model simulation results by vegetation types and geographic regions to assess changes in SOC and C fluxes over time. Trend significance and slope of the time series data (GPP, NEE, and SOC) were calculated using a non-parametric Mann-Kendall test that detects monotonic upward or downward trends (Yue et al., 2002). The test was implemented in R with the “zyp” package (Bronaugh et al., 2023) and applied to both individual Ameriflux/NEON sites and vegetation groups (Table S8 in Supporting Information S1). We also computed the correlation between site-based 20-year change in SOC stocks and climate, soil, and topographic variables (Table 1) to identify regional controlling factors for model-simulated SOC sequestration in rangelands.

3. Results

3.1. Model Accuracy for Estimating Rangeland Productivity

We used GPP to assess the performance of the RCTM's ability to estimate rangeland productivity. Overall, we found that the resulting daily GPP model estimates for the grass-shrub vegetation group had the best agreement with flux tower-derived GPP ($R^2 = 0.70$, $RMSE = 0.9 \text{ g C m}^{-2} \text{ day}^{-1}$), followed by the grass-tree mixture ($R^2 = 0.60$, $RMSE = 1.1 \text{ g C m}^{-2} \text{ day}^{-1}$). Whereas agreement for the perennial and/or annual grass sites ($R^2 = 0.58$, $RMSE = 2.2 \text{ g C m}^{-2} \text{ day}^{-1}$) was somewhat lower (Figure 3). The perennial and/or annual grass-specific model obtained $R^2 = 0.69$ and $RMSE = 3.1 \text{ g C m}^{-2} \text{ day}^{-1}$ for estimating daily GPP from the two sites identified as managed hay and pasture.

Using LOOCV, RCTM was shown to have similar R^2 values of ~ 0.60 across all vegetation classes (Table 2). The MBE values revealed a slight underestimation of GPP in the model outputs compared to flux tower-derived estimates. This type of underestimation was the most pronounced for higher GPP values (Figure S6 in Supporting Information S1), while model overestimation occurred more frequently for GPP values below $1 \text{ g C m}^{-2} \text{ day}^{-1}$, especially for the perennial and/or annual grass and the grass-shrub sites (Figures 3a and 3c). Both MBE and RB values indicated pronounced bias for modeling GPP from grass-tree sites (Table 2). In particular, the Mpj site appears to have a higher bias compared to other sites (Figure 3d), likely due to its high percentage of tree coverage.

The modeling bias was also high for several individual Ameriflux (e.g., Bkg, Var) and NEON (e.g., xKA) sites within the perennial and annual grass category (Figure 3a), which can be attributed to the challenges of modeling C response under heterogeneous and/or disturbed conditions, including grazing (Bkg, Var), mixed grass species (Bkg), and the presence of crops (xKA) on rangeland productivity using RCTM.

Model performance for estimating rangeland productivity represented by GPP was strongly impacted by the seasons (Figures 4a and 4c). During the summer season (S2 and S3), model performance was significantly higher ($R^2 = 0.5\text{--}0.7$) for all vegetation types compared to the winter season (S1, with $R^2 < 0.4$ for perennial/annual grasses and grass-shrub mixture sites) (Figure 4a). The best model fit was achieved between June and August for perennial and/or annual grass and grass-tree mixture sites, while grass-shrub mixture sites had a similar model fit for March to May and June to August. However, it should be mentioned that the model RMSE (Figure 4c) was also noticeably higher during the summer season because winter GPP values were lower in magnitude than those during the summer season. When looking at normalized RMSE or RB, the results were not as different across seasons for grass-shrub and grass-tree mixture sites (Table S5 in Supporting Information S1).

The annual cumulative GPP estimates were more accurate for grass-shrub mixture ($R^2 = 0.73$, $RMSE = 198 \text{ g C m}^{-2} \text{ year}^{-1}$) than for the grass-tree mixture ($R^2 = 0.68$, $RMSE = 383 \text{ g C m}^{-2} \text{ year}^{-1}$) or perennial and/or annual grass ($R^2 = 0.61$, $RMSE = 332 \text{ g C m}^{-2} \text{ year}^{-1}$) sites, which is consistent with model

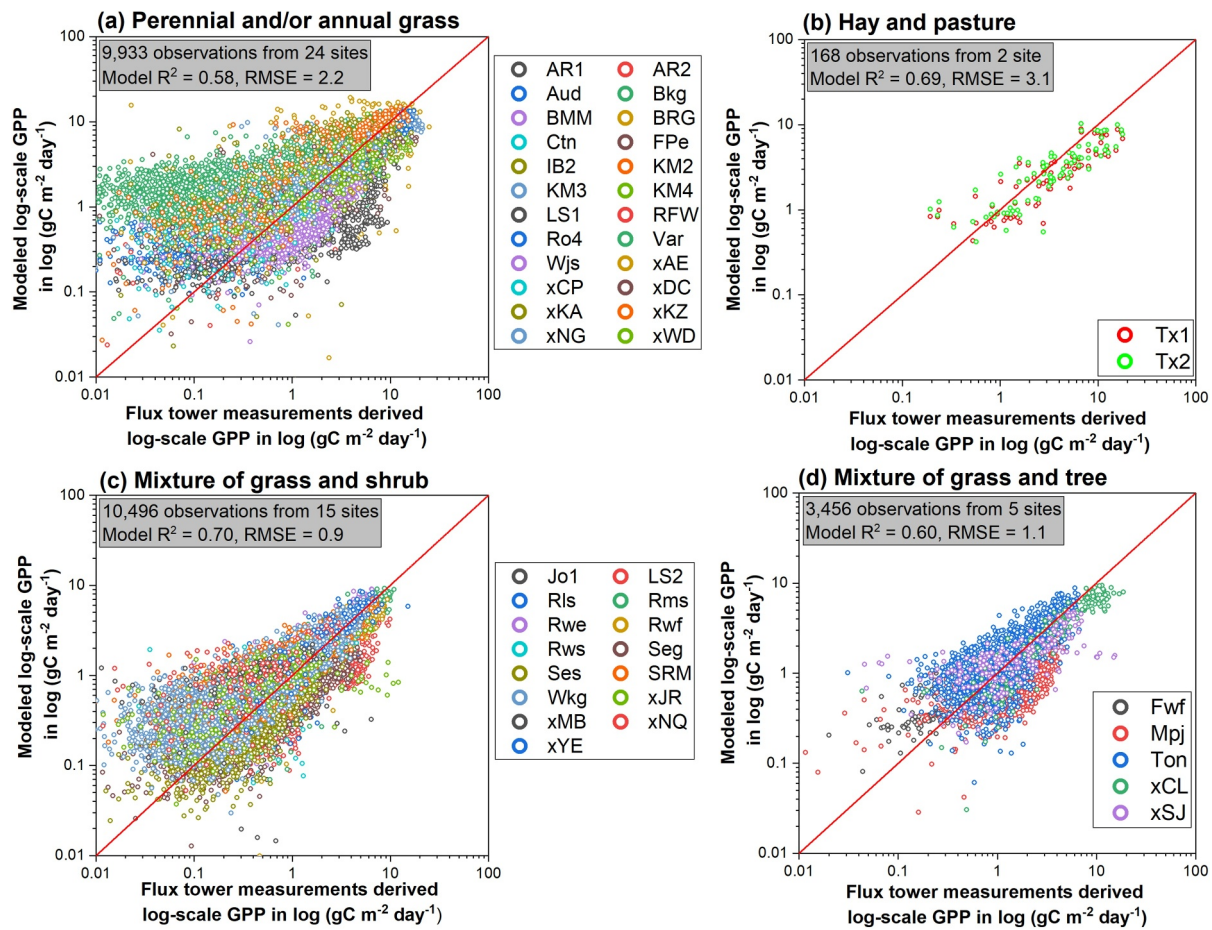


Figure 3. Model fit for gross primary productivity (GPP) represented by the coefficient of determination (R^2) and root mean square error (RMSE, $\text{g C m}^{-2} \text{ day}^{-1}$) for different vegetation classes, including (a) perennial and/or annual grass, (b) managed hay and pasture, (c) mixture of grass and shrub, and (d) mixture of grass and tree classes. The plot is displayed on a logarithmic scale, with different colors representing different study sites.

performance ranking for estimating daily GPP (Figure 3). Despite the markedly better model fit (R^2) in estimating daily GPP during the summer season, cumulative GPP estimates from April to October showed similar accuracy compared to annual estimates, indicating that model bias might be reduced when integrating results from the summer and non-summer seasons. The model bias (MBE = $-139 \text{ g C m}^{-2} \text{ year}^{-1}$; RB = -0.13) was larger for the estimates of annual GPP for grass-tree mixture sites (Table 3). This significant underestimation is probably due to the higher complexity of the grass-tree system and the smaller number of sites with available observations. The model performance for estimating monthly cumulative GPP was similar among different vegetation types, with R^2 over 0.7 (Table 3). Again, the model bias, indicating an underestimation of GPP, was higher for the monthly estimates from the grass-tree mixture sites.

3.2. Model Accuracy for Estimating Net Rangeland C Fluxes and SOC Stocks

3.2.1. Model Accuracy for Estimating Rangeland NEE

When including all sites at the 5-day timestep, the RCTM system yielded better model NEE performance for the grass-shrub mixture ($R^2 = 0.47$, RMSE = $0.6 \text{ g C m}^{-2} \text{ day}^{-1}$) relative to the grass-tree mixture ($R^2 = 0.37$, RMSE = $0.8 \text{ g C m}^{-2} \text{ day}^{-1}$) sites and the perennial and/or annual grass ($R^2 = 0.27$, RMSE = $1.6 \text{ g C m}^{-2} \text{ day}^{-1}$) sites (Figure 5). Daily NEE from the managed hay and pasture sites were estimated with limited accuracy using the perennial and/or annual grass-specific model ($R^2 = 0.21$, RMSE = $2.1 \text{ g C m}^{-2} \text{ day}^{-1}$). The model bias was particularly large for xCL (grass-tree mixture site with grazing) and KLS (perennial site with some data gaps), with the model struggling to predict the really high observed NEE values at these sites. The LOOCV results

Table 2

Gross Primary Productivity (GPP, $\text{g C m}^{-2} \text{ Day}^{-1}$) and Net Ecosystem Exchange of CO_2 (NEE, $\text{g C m}^{-2} \text{ Day}^{-1}$) Model Performance Shown as Coefficient of Determination (R^2), Root Mean Square Error (RMSE), Normalized Root Mean Square Error (nRMSE), Mean Bias Error (MBE), and Relative Bias (RB) Averaged for Different Vegetation Classes

Error metric ^a	Perennial and/or annual grass		Grass-shrub mixture		Grass-tree mixture	
	Model fit	LOOCV	Model fit	LOOCV	Model fit	LOOCV
GPP models						
R^2	0.58	0.62 ± 0.20	0.70	0.62 ± 0.25	0.60	0.59 ± 0.26
RMSE	2.19	2.07 ± 1.27	0.84	1.04 ± 0.54	1.08	1.77 ± 0.88
nRMSE	0.83	0.76 ± 0.28	0.74	0.78 ± 0.41	0.60	0.79 ± 0.25
MBE	-0.03	-0.10 ± 0.92	-0.03	-0.01 ± 0.65	-0.21	-0.47 ± 1.20
RB	-1.1	-0.8 ± 32.5	-2.4	9.5 ± 42.1	-11.9	-13.2 ± 53.8
NEE models						
R^2	0.27	0.32 ± 0.22	0.47	0.45 ± 0.19	0.37	0.38 ± 0.20
RMSE	1.57	1.45 ± 0.69	0.64	0.69 ± 0.34	0.82	1.04 ± 0.70
nRMSE	5.33	4.88 ± 75.6	3.32	5.01 ± 4.84	5.91	-0.44 ± 4.11
MBE	-0.27	-0.29 ± 0.38	-0.15	-0.21 ± 0.32	-0.13	-0.31 ± 0.57
RB	-90.6	-133.1 ± 267.2	-75.3	-33.6 ± 120.6	-91.9	-97.4 ± 19.1

Note. Both model fits and leave-one-out cross-validation (LOOCV) results are presented.

^a R^2 = coefficient of determination; RMSE = root mean square error; nRMSE = normalized root mean square error; MBE = mean bias error; RB = relative bias.

(Table 2) also suggest the need to further improve the NEE models, especially for the perennial and/or annual grass sites ($R^2 = 0.32$, $\text{MBE} = 0.3 \text{ g C m}^{-2} \text{ day}^{-1}$).

Overall, the model fit was observed to be better for the summer and shoulder seasons than for winter NEE estimates (R^2 difference is about 0.1–0.2), except for grass-tree mixture sites (Figure 4b). For perennial and/or annual grass sites, model RMSE was higher for the summer and shoulder seasons than for winter (Figure 4d). Even though the RCTM system showed limited success in estimating daily NEE flux (Figure 5), the model performance was better for estimating monthly (R^2 between 0.4 and 0.6), summer and shoulder seasons cumulative (R^2 between 0.4 and 0.7), or annual cumulative (R^2 between 0.4 and 0.7) NEE fluxes (Table 3). Especially, R^2 improved by 126%, 55%, and 84% for perennial and/or annual grass, grass-shrub mixture, and grass-tree mixture sites, respectively, when aggregating results from daily to annual cumulative.

3.2.2. Model Accuracy for Estimating Rangeland RECO

When evaluating RECO at the 5-day timestep, the overall model performance was relatively strong for perennial and/or annual grass ($R^2 = 0.6$; $\text{RMSE} = 1.5 \text{ g C m}^{-2} \text{ day}^{-1}$), hay and pasture ($R^2 = 0.62$; $\text{RMSE} = 1.7 \text{ g C m}^{-2} \text{ day}^{-1}$) and grass-shrub mixture sites ($R^2 = 0.64$; $\text{RMSE} = 0.6 \text{ g C m}^{-2} \text{ day}^{-1}$; Figure S9 in Supporting Information S1). Whereas grass and tree sites had a lower overall performance with an R^2 of 0.38, which was mostly driven by the Ton site, which has a significant presence of evergreen and is periodically grazed.

The model performance was moderate (R^2 between 0.6 and 0.7) for estimating cumulative annual or monthly RECO (Table S7 in Supporting Information S1). The monthly model R^2 performance for RECO increased by 22% for perennial and/or annual grass, by 5% for grass-shrub mixture sites, and 74% for grass-tree mixture sites (Table 3). The large improvement in RECO performance when shifting from a 5-day average to monthly cumulative timestep indicates that there are seasonal weaknesses in the model, probably due to decreased uncertainty when aggregating temporal data sets.

The cumulative RECO model performance was similar to that reported for GPP models and was therefore better than NEE models (Table 3). It was anticipated that the model performance should be lower for NEE than for GPP or RECO, considering that the model structure for estimating NEE is subject to uncertainty in simulating both

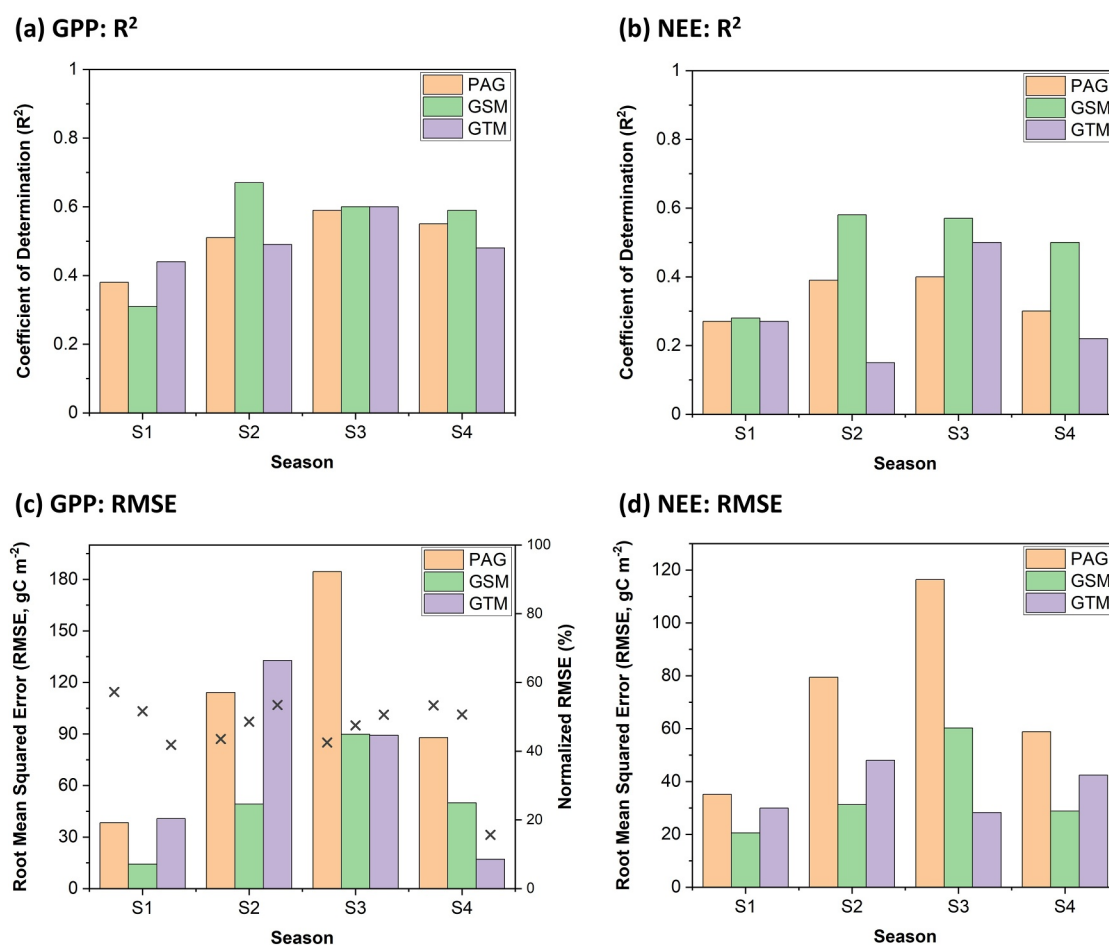


Figure 4. Model performance for estimating (a) gross primary productivity (GPP) represented by coefficient of determination (R^2), (b) net ecosystem exchange of CO_2 (NEE) represented by R^2 , (c) GPP represented by root mean square error (RMSE, C m^{-2} per seasonal cumulative), and (d) NEE represented by RMSE. The results are averaged from sites grouped by four seasons, including S1 (December, January, February), S2 (March, April, May), S3 (June, July, August), and S4 (September, October, November). The model performance is presented for perennial and/or annual grass (PAG) sites, grass and shrub mixture (GSM) sites, and grass and tree mixture (GTM) sites.

grassland production and RECO and that GPP and RECO might not have equivalent responses to climate conditions such as soil moisture and temperature. Regardless of the temporal resolution (i.e., daily or cumulative) used for model performance evaluation, the RCTM performed consistently better for grass-shrub mixture sites.

3.2.3. Model Accuracy for Estimating Rangeland SOC Stocks

The model-simulated surface SOC stocks agreed well with SOC measurements from NEON sites ($R^2 = 0.58$, Figure 6), especially considering how difficult SOC is to model in natural systems. However, the model simulation results were higher than the observed 0–30 cm SOC stocks ($\text{MBE} = 2,535 \text{ g m}^{-2}$). This is because RCTM inputs are not restricted to a specific depth layer (e.g., 30 cm) but are instead reflective of the integrated plant productivity signals due to the use of GPP and NEE data for model calibration. However, the RCTM-simulated SOC stocks were significantly lower than those observed from the 0–100 cm depth ($\text{MBE} = -7,293 \text{ g m}^{-2}$, Figure S10 in Supporting Information S1), meaning that SOC stocks from 0 to 100 cm were too deep for RCTM to capture. The exact soil depth that the models can capture varies greatly between sites because rooting depths vary as a function of plant community composition, soil type, and moisture regimes (Schenk & Jackson, 2002). The vertical C transport processes that redistribute C deeper into the solum also vary by order of magnitude across ecosystems (Heimsath et al., 2005).

Table 3

Model Performance for Estimating Annual, Seasonal, and Monthly Cumulative Gross Primary Productivity (GPP) and Net Ecosystem Exchange of CO₂ (NEE) Shown as Coefficient of Determination (R^2), Root Mean Square Error (RMSE), Normalized Root Mean Square Error (nRMSE), Mean Bias Error (MBE), and Relative Bias (RB) Averaged From Sites Within Different Vegetation Types

Vegetation class	GPP						NEE					
	Mean	R^2	RMSE	nRMSE	MBE	RB	Mean	R^2	RMSE	nRMSE	MBE	RB
Annual cumulative fluxes (g C m ⁻² year ⁻¹)												
Perennial and/or annual grass	1096	0.61	331.5	0.33	-16.2	-0.01	105	0.53	176.1	-0.96	-102.7	-1.46
Grass-shrub mixture	498	0.73	198.3	0.38	-21.6	0.05	66	0.67	100.9	1.00	-78.4	-0.66
Grass-tree mixture	659	0.68	383.0	0.50	-138.5	-0.13	55	0.42	174.9	0.21	-100.3	-1.03
Summer season cumulative fluxes (g C m ⁻² per summer season)												
Perennial and/or annual grass	748	0.55	258.4	0.37	-7.4	0.01	121	0.45	155.5	0.45	-72.3	-0.93
Grass-shrub mixture	352	0.72	146.3	0.39	-18.5	0.05	81	0.69	93.6	0.56	-68.0	-0.33
Grass-tree mixture	432	0.71	260.4	0.47	-98.1	-0.06	60	0.40	120.7	0.86	-50.6	-0.11
Monthly cumulative fluxes (g C m ⁻² month ⁻¹)												
Perennial and/or annual grass	79	0.72	50.0	0.68	-2.2	0.002	9	0.42	34.2	0.47	-8.6	-0.78
Grass-shrub mixture	34	0.73	26.2	0.70	-0.8	0.04	6	0.58	17.2	2.5	-6.6	-0.67
Grass-tree mixture	52	0.70	44.9	0.70	-12.8	-0.14	4	0.46	24.5	-0.1	-9.0	-0.99

Note. The summer season, including part of the shoulder season, is set from April to October for comparison. Mean values are also calculated for different categories.

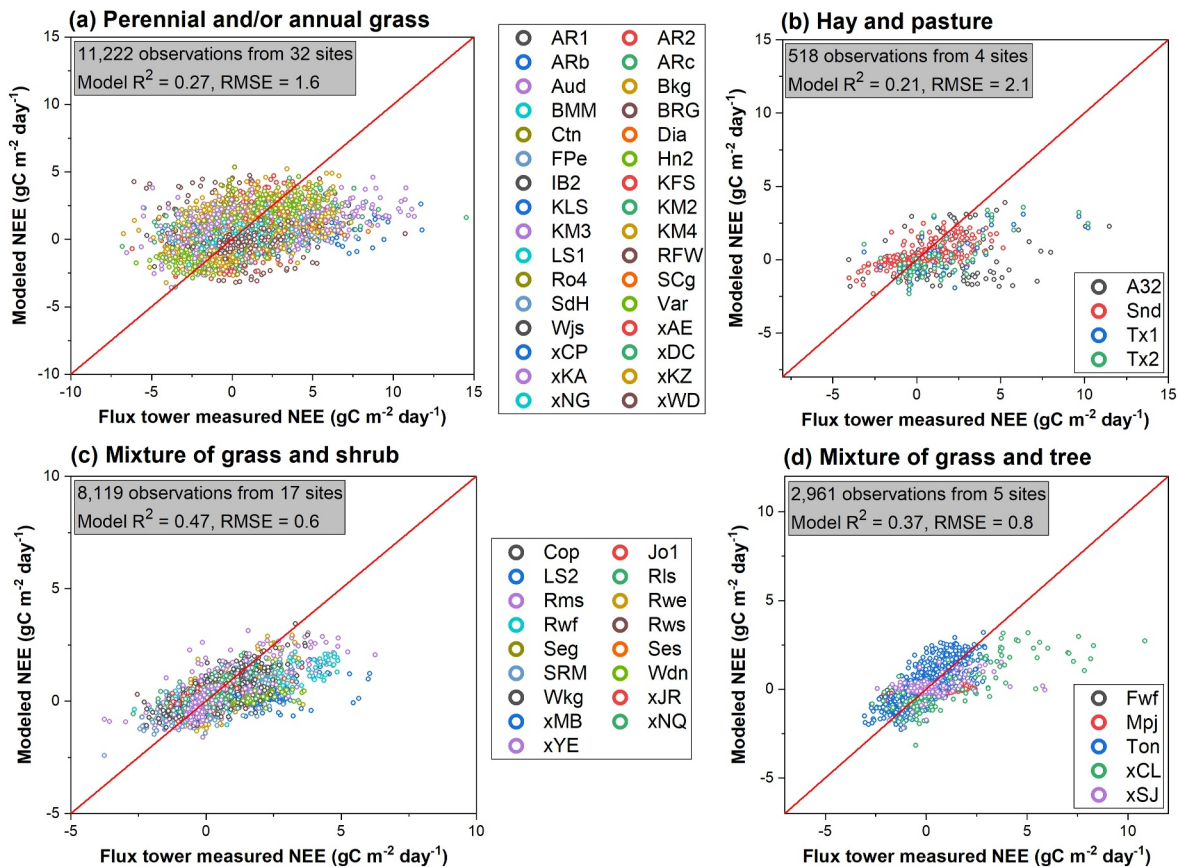


Figure 5. Model fit for net ecosystem exchange of CO₂ (NEE) represented by the coefficient of determination (R^2) and root mean square error (RMSE, C m⁻² day⁻¹) for different vegetation classes including (a) perennial and/or annual grass, (b) managed hay and pasture, (c) mixture of grass and shrub, and (d) mixture of grass and tree classes. Positive NEE sign denotes ecosystem carbon sink activity. Different colors represent different study sites.

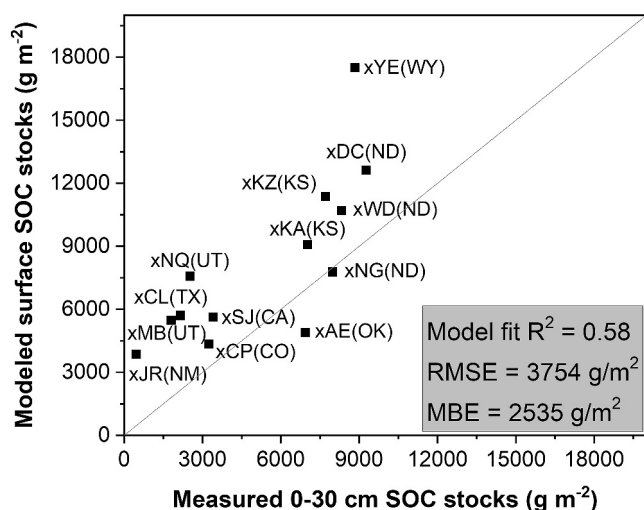


Figure 6. The model performance for estimating surface soil organic carbon (SOC) stocks for NEON grassland sites using the calibrated Rangeland Carbon Tracking and Management (RCTM) system.

3.3. Rangeland C Dynamics Influenced by Site and Environmental Factors

The RCTM-simulated annual cumulative GPP was strongly correlated with both surface ($R = 0.7$) and root zone soil moisture ($R = 0.8$), VPD ($R = -0.4$), and fPAR ($R = 0.9$) (Table 3). Significant linear correlations were observed between simulated annual average SOC and VPD ($R = -0.4$), soil temperature ($R = -0.4$), and fPAR ($R = 0.6$). The RCTM simulation also suggested significant relationships between RECO and all of the input variables investigated ($P < 0.05$), with fPAR (0.56), VPD (-0.44), soil temperature (-0.44), and SOC (0.42) yielding the strongest correlations. The annual cumulative NEE was less correlated with individual environmental variables used in the model ($R < 0.2$), which might be explained by the close to steady-state conditions of the sites and the absence of linear relationships. As expected, model-simulated SOC was significantly correlated with both GPP (0.41) and RECO (0.42) ($P < 0.05$).

3.4. Temporal Changes in C Fluxes and SOC Stocks

Simulations were carried out to explore temporal patterns of C fluxes and SOC over the period from 2003 to 2022 that were influenced by vegetation types and geographic regions. Both GPP and SOC stocks showed an

increasing trend for Ameriflux and NEON sites grouped in perennial and/or annual grass, managed hay and pasture, and grass-shrub mixture classes (Figure 7). According to model simulation results, surface SOC stocks increased by 4.7, 6.2, and 8.4 $\text{g C m}^{-2} \text{ year}^{-1}$, for perennial and/or annual grass, managed hay and pasture, and grass-shrub mixture sites, respectively (Table S8 in Supporting Information S1). Similar temporal trends showing an increase in SOC stocks (i.e., SOC sequestration) were found when grouping the sites into USDA agricultural regions (Cooter et al., 2012), including the Northern Great Plains (6.2 $\text{g C m}^{-2} \text{ year}^{-1}$), the Southern Great Plains (6.2 $\text{g C m}^{-2} \text{ year}^{-1}$), the Mountain regions (6.7 $\text{g C m}^{-2} \text{ year}^{-1}$), and the Midwest (10 $\text{g C m}^{-2} \text{ year}^{-1}$), which are tied to an increase in GPP over time (Figure S11 in Supporting Information S1). For individual Ameriflux/NEON sites, RCTM simulated a significant ($P < 0.05$) increase in surface SOC stocks for 69% of the sites, with a smaller percentage (13%) associated with SOC decrease (Table S8 in Supporting Information S1). While a GPP increase was simulated for 80% of the sites, the increase was found to be significant for only 16% of the sites. The most significant increases (at a rate of 12–22 $\text{g C m}^{-2} \text{ year}^{-1}$) were found in Kellogg Biological Station sites in Michigan.

4. Discussion

4.1. RCTM Model Performance Compared to Previous Work

In comparison to previous research estimating broad-scale rangeland productivity, our GPP model demonstrated similar or better performance. For example, Jin et al. (2020) carried out a vegetation type-specific model calibration for the Mongolian Plateau, achieving a model performance of $R^2 = 0.57$ in estimating grassland NPP, which is comparable to RCTM. L. X. Zhang et al. (2015) compared four LUE-type models with varying complexity and found less accurate model estimations for grasslands (R^2 between 0.45 and 0.64; RMSE between 1.9 and 2.6 $\text{g C m}^{-2} \text{ day}^{-1}$) compared to croplands (R^2 between 0.59 and 0.73) using a global flux tower data set. In addition, using a global flux tower data set, Zhu et al. (2018) examined MODIS GPP products, which were also developed based on the LUE-type algorithms. Their study found moderate model fit ($R^2 = 0.66$) but relatively large RMSE (2.5 $\text{g C m}^{-2} \text{ day}^{-1}$), as well as a bias indicating an underestimation of grassland GPP. Work by F. Zhang et al. (2012) reported a model accuracy of $R^2 = 0.74$ for estimating annual GPP using the MODIS LUE algorithm when tested against an earlier and smaller flux tower data set from US grasslands. Calibrated against both Ameriflux and EuroFlux network sites, the work of Yuan et al. (2007) demonstrated better model performance than ours ($R^2 = 0.77$), which may be explained by the fact that their data set included not only grassland but also savanna and forest sites, allowing the LUE algorithms to better capture broader-scale climate and vegetation driving factors.

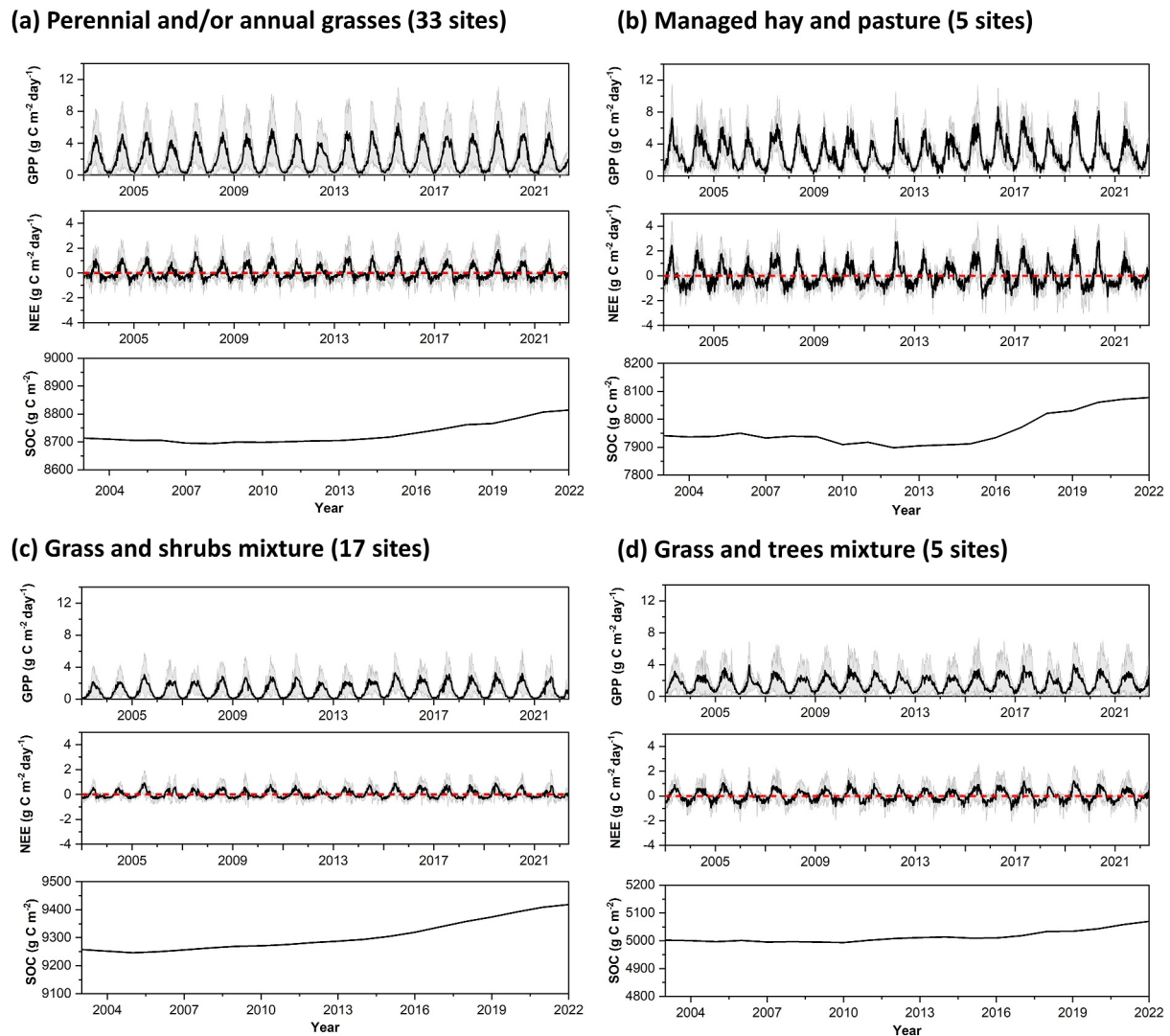


Figure 7. Model estimated temporal trends (2003–2022) in gross primary productivity (GPP), net ecosystem exchange (NEE), and surface soil organic carbon (SOC) stocks grouped by vegetation classes including (a) perennial and annual grass, (b) managed hay and pasture, (c) mixture of grass and shrub, and (d) mixture of grass and tree classes. The solid lines represent mean values averaged from all sites within the group, while the lighter-colored lines with areas filled within represent standard deviations for GPP and NEE estimates. The red line shows zero baseline for NEE where a positive NEE denotes ecosystem carbon sink activity. Different scales were used for SOC due to differences in data ranges among vegetation types.

In contrast to the extensive modeling efforts dedicated to rangeland GPP estimation, there have been limited research efforts on modeling rangeland NEE and SOC, especially with the use of an RS-driven, process-based modeling approach like the RCTM system. We performed a comparison between RCTM and L4C (Endsley et al., 2020) using the Ameriflux/NEON sites (Text S2, Tables S9, and S10 in Supporting Information S1) and found that RCTM outperformed L4C results in terms of NEE estimates for perennial and/or annual grass and grass-shrub mixture sites, while the performance was similar for grass-tree mixture sites (Table S10 in Supporting Information S1). This is not surprising because, in the global L4C land-cover map, the single “Grasslands” vegetation type (i.e., plant functional type) represents fairly diverse bioclimatic settings. The L4C parameters were calibrated using a global FLUXNET data set that may not necessarily capture the interactions between climate factors and rangeland soil dynamics within a smaller region. Another explanation is that the STARFM fPAR inputs, calculated at 30 m resolution, utilized by RCTM can match tower footprints and capture management-associated changes in rangeland C dynamics.

Table 4

Correlation Among Model Estimated Annual Cumulative Net Ecosystem Exchange (NEE), Gross Primary Productivity (GPP), Ecosystem Respiration (RECO), Annual Average Soil Organic Carbon (SOC) Stocks, and Model Input Variables Including 0–5 cm Soil Moisture (SWC_sf), Root Zone Soil Moisture (SWC_rt), Vapor Pressure Deficit (VPD), 0–5 cm Soil Temperature (ST), Clay Content (Clay), and Fraction of Absorbed Photosynthetically Active Radiation (fPAR)

	NEE	GPP	RECO	SOC	SWC_sf	SWC_rt	VPD	ST	Clay	fPAR
NEE	1									
GPP	0.26*	1								
RECO	0.15	0.99*	1							
SOC	−0.01*	0.41*	0.42*	1						
SWC_sf	0.14*	0.70*	0.19*	0.19*	1					
SWC_rt	0.15*	0.78*	0.25*	0.25*	0.97*	1				
VPD	−0.14*	−0.44*	−0.44*	−0.44*	−0.66*	−0.60*	1			
ST	−0.04	0.10*	−0.44*	−0.44*	−0.23*	−0.16*	0.71*	1		
Clay	0.01	0.09*	−0.01*	−0.01	0.10*	0.11*	0.09*	0.17*	1	
fPAR	0.20*	0.88*	0.56*	0.56*	0.62*	0.62*	−0.50*	−0.07*	−0.03	1

Note. * The correlation is significant at $P < 0.05$.

Accurately estimating the small net change in two large fluxes (GPP and RECO) is a difficult task that nearly all process-based models currently struggle to do well. Abdalla et al. (2013) used the DNDC model to simulate C dynamics within Irish grasslands and reported a model performance for estimating monthly cumulative C fluxes ($R^2 = 0.51$) that is comparable to ours. The modeling work of Sándor et al. (2016) showed that both the biome-generic Biome-BGC ($R^2 = 0.28$) and the grassland-specific Pasture Simulation model ($R^2 = 0.42$) had limited model accuracy for estimating weekly NEE from European grassland sites, despite a higher model performance reported for GPP estimates ($R^2 > 0.75$). Limited accuracy was reported for simulating RECO from grassland sites using the CENTURY model, unless a time-lag factor was considered to account for legacy climate impacts (Kelly et al., 2000). Regarding SOC, L. Zhang et al. (2007) and Y. Zhang et al. (2007) reported that CENTURY-simulated surface SOC stocks agreed well ($R^2 = 0.68$) with measurements at Qinghai-Tibetan Plateau sites. It should be noted that the variations in model performance between RCTM and these two studies may be attributed to differences in geographic coverage.

4.2. Factors Driving Regional Rangeland C Dynamics

The strong correlation between GPP and fPAR, as well as GPP and RECO, highlights the interconnected nature of vegetation growth and C fluxes (Table 4). However, this strong correlation may also indicate that the RCTM-based simulation of rangeland C dynamics is highly sensitive to model inputs related to vegetation growth, such as soil moisture and fPAR. Therefore, both the quality of model inputs, as well as their influence on the interconnected model outcomes require further examination. The temporal trends observed for GPP and SOC changes are strongly controlled by the pattern observed in the RS-informed fPAR values. In perennial and/or annual grass, managed hay and pasture, and grass-shrub mixture sites, GPP and SOC remained relatively constant until 2013 and then began to increase (Figure 7). A similar trend was found for most of the regional-level summaries (Figure S11 in Supporting Information S1), which aligned with fPAR changes shown in Figure S12 in Supporting Information S1. The fPAR values are often used to represent vegetation greenness (Forkel et al., 2014; Twine & Kucharik, 2008). In this context, rangeland greenness can be influenced both by environmental conditions and management practices (Browning et al., 2019; Long et al., 2019; Shibia et al., 2022).

The annual average fPAR correlated strongly ($R > 0.6$) with soil moisture (Table 3), which is in line with the significant correlations ($R > 0.5$, $P < 0.05$) computed between fPAR and annual precipitation at the regional scale (Figure S12 in Supporting Information S1). Our simulation results suggest that increased rangeland greenness was often associated with higher annual precipitation levels, particularly at the grass-shrub mixture and grass-tree mixture sites. This finding is consistent with previous work that reported enhanced rangeland productivity in wetter years (Golodets et al., 2013; Liu et al., 2021; Scott et al., 2023). A strong correlation ($R = 0.64$) was also found between fPAR and air temperature for perennial and/or annual grass sites; however, this correlation was

less certain for other sites involving trees or shrubs, or when results are aggregated at the regional scale (Figure S12 in Supporting Information S1). The uncertainty may stem from enhanced vegetation metabolism, increased SOC decomposition, and a prolonged growing season linked to higher temperatures, but is reversed by plant growth inhibition induced by heat or water stress (Izaurrealde et al., 2011). In addition, vegetation composition (e.g., C3 vs. C4) and ecoregion can often influence the magnitude and direction of climate effects on rangeland productivity and C dynamics (Fuhlendorf et al., 2000; Hossain & Li, 2021).

Conservation practices such as prescribed grazing management, grassland restoration, and removal of invasive species can enhance rangeland greenness through the promotion of vegetation growth, increased biodiversity and resilience, reduced risks of wildfires, and improved water supply (Rolfe et al., 2021; Schmelzer et al., 2014; Silverman et al., 2019); whereas, practices that lead to rangeland degradation can cause reduced rangeland greenness (Paudel & Andersen, 2010; Smet & Ward, 2005). Unfortunately, distinguishing management effects from climate variability on rangeland greenness can be challenging (L. Li et al., 2018), especially when there is a lack of detailed temporal information of grazing management (i.e., timing, intensity, and duration) and vegetation composition from most of the sites. Running the RCTM at a 30 m spatial resolution will be useful to identify local areas of change in C dynamics. Ideally, assessing long-term changes in rangeland productivity and SOC from reference sites, alongside sites undergoing practice changes, would more effectively capture the influence of these practices on rangeland C dynamics.

Environmental drivers are crucial not only for overall SOC stock levels (Table 4) but also for changes in SOC stocks. Our regression analysis (Text S3 in Supporting Information S1) estimated higher SOC sequestration rates for soils with higher clay contents, which can potentially be explained by the ability of finer-textured soils to better protect SOC from decomposition through physical protection and chemical adsorption (Blanco-Canqui and Lal, 2004; Hassink, 1997; Huys et al., 2022; Mao et al., 2024). If these model estimates are confirmed with observational data, grassland management should prioritize clay-rich soils for practices that enhance C inputs, improve water capacity, reduce erosion, and optimize grazing intensity. These efforts would better facilitate organic matter stabilization and maximize C sequestration benefits. However, the linear correlation between model-simulated SOC stocks and clay contents was not significant (Table 4), which somewhat contradicts the modeled temporal changes. This suggests that the role of soil texture as a primary driving factor of C sequestration remains uncertain. Further research is required to clarify this relationship and account for potential confounding factors, such as variations in management practices, climatic conditions, and vegetation types, which may obscure the influence of soil texture. Likewise, several environmental factors were highly correlated with SOC stocks but not with SOC stock changes according to LASSO regression results (Text S3 in Supporting Information S1). Further investigation using long-term SOC measurement data is needed to confirm the controlling factors identified through our modeling study.

4.3. Limitations and Future Work

While the RCTM model performed well overall, uncertainties remain that warrant further investigation. The discrepancy in modeled and measured SOC stocks points to the need to further refine RCTM to account for the diffusion and advection among different depth layers (Sanderman & Amundson, 2008; Y. Zhang et al., 2021) as well as the depth effects on SOC decomposition. However, for outcome-based monitoring of SOC sequestration, the important data is the net flux over time, which for the RCTM as currently calibrated has a conservative bias (Table 3). The use of average environmental conditions from a relatively short period of time for model initialization, along with the fact that RS inputs and NLDAS-based soil moisture and temperature data might not fully capture management (e.g., irrigation) or legacy climate impacts on SOC dynamics (Delgado-Baquerizo et al., 2017; Nie et al., 2022), might also lead to estimation bias. It should be noted that RCTM or similar RS-driven process modeling approach-based systems may be limited by the ability of RS inputs to adequately capture management-driven (e.g., grazing, irrigation) changes in rangeland greenness. This may be greatly influenced by the spatial resolution and temporal repeat of the RS detection, as well as the sensor/wavelengths being used to track vegetation and other ecosystem properties. Future work should verify RCTM-simulated long-term trends in rangeland productivity with long-term biomass monitoring data sets. Simulating a historic run-in period using a longer-term record, as done with some activity-based models (e.g., Hartman et al., 2011), may help eliminate this bias.

It would also be worthwhile to directly compare RCTM with activity-data driven models, such as DNDC (C. Li et al., 1994) and DAYCENT (Parton et al., 1998) to assess their accuracy and uncertainty in predicting the spatial and temporal rangeland C dynamics. In particular, the LUE algorithms used by RCTM may not fully capture the management effects on actively grazed or hayed sites. Therefore, a comparison with activity-data driven models could help identify areas for improvement in RS-driven models like RCTM. Moreover, our modeling results found that RCTM had a relatively large modeling bias for estimating GPP from grass-tree mixture sites (Figure 3), which might be associated with signal saturation in RS data caused by dense vegetation (Huete & Jackson, 1988; Zhu & Liu, 2015). The use of saturation or cloud-adjusted indices, as well as a combination of vegetation indices may be necessary to improve the accuracy of modeling the grass-tree mixture sites (Badgley et al., 2019; Gu et al., 2013; Yang et al., 2012). Also tied to RS inputs, the relatively lower model fit observed in the estimation of non-summer GPP and NEE (Figures 4a and 4b) might be explained by the fact that the STARFM fusion method is constrained by a reduced number of Landsat and MODIS images and pixels passing the QC criteria during this period. This underscores the need to better account for snow cover effects and implement noise-reduction techniques in the case of missing data (Cao et al., 2018; Huang et al., 2021). Furthermore, the modeling bias for estimating NEE (Figure 5) and SOC (Figure 6) is significant, as reflected by the deviation of measured versus modeled values from the 1:1 line. These results suggest that the estimates from the current RCTM version are less accurate at the lower and higher ends, pointing to the need for further model parameterization, evaluation, and uncertainty analysis using data sets that cover a wider range of environmental and management conditions. Moreover, the notably higher modeling bias observed in grassland sites compared to grass-shrub sites highlights the model's greater ability to capture variability associated with generalized vegetation types rather than the finer distinctions within each class. This is perhaps because RS signals are more effective at detecting differences in shrub presence within grassland sites than capturing subtle variations in vegetation characteristics, which requires future testing with better vegetation information at each model calibration and validation site. Additionally, the wide range of management practices in grassland sites, such as mowing, irrigation, and grazing with varying timing and intensity, may have further complicated the modeling of rangeland productivity and C dynamics. This challenge is associated with RCTM's reliance on RS signals rather than directly incorporating management information.

There are several improvements in model parameterization that we believe can further increase the accuracy and applicability of RCTM. First, more accurate model input and parameter estimates can be used, such as footprints calculated by Chu et al. (2021) and estimates of root:shoot ratios that are expressed as a function of climate factors (e.g., temperature, precipitation) and vegetation types (Hui & Jackson, 2006; Qi et al., 2019; C. Wang et al., 2021), for allocating modeled NPP into aboveground and belowground biomass. Parameterizing the RCTM for more detailed vegetation types such as annual versus perennial grass (Milne & Haynes, 2004), C3 versus C4 grass (L. Zhang et al., 2007; Y. Zhang et al., 2007), tallgrass versus shortgrass (Pepper et al., 2005), and pastures with different qualities (de Oliveira et al., 2022) that are known to have varying vegetation growth and C dynamics (Guerschman et al., 2003; Otunga et al., 2019; C. Wang et al., 2014) may also help improve model performance. Even though the algorithms for estimating LUE and C dynamics have been thoroughly developed in SMAP's L4C model (Endsley et al., 2020), adapting such algorithms to estimate vegetation group-specific parameters for grasslands can be associated with large uncertainty, which is reflected in our model calibration results (Figures S4 and S5 in Supporting Information S1). This calls for the need to better constrain the parameter space by utilizing a larger number of calibration sites and a better estimate of the priors of the parameters, coupled with the identification of effective sample size for model calibration and validation using the MCMC algorithm.

Future work should also examine the ability of RCTM or other RS-driven models to capture the effects of management practices (e.g., grazing and irrigation) and ecological disturbances (e.g., drought, fire) on vegetation growth (Hao & He, 2019; Su et al., 2022), litter quality (J. Gao et al., 2020), and SOC dynamics (Conant et al., 2017; McSherry & Ritchie, 2013; Sanderson et al., 2020). Combining RCTM with activity-driven algorithms is hypothesized to improve model performance and applicability to managed livestock operations, which warrants further investigation. For example, the DNDC-type algorithms (C. Li et al., 2012) can be incorporated to better describe the conversion from animal ingested biomass into manure and the partition of manure into SOC pools. Model calibration and validation, along with the determination of reference values or thresholds for model initialization, should be further strengthened by taking advantage of emerging, network-based data sets that reflect long-term changes in vegetation biomass, SOC stocks, and C fluxes (Bond-Lamberty et al., 2020; Chang et al., 2015; Moll-Mielewicz et al., 2023). Finally, the RCTM needs to be further evaluated and improved for

site-level estimates of rangeland productivity and C dynamics (Text S4, Figures S13–S15, Tables S11, and S12 in Supporting Information S1) in order to inform management decisions. This can be achieved by utilizing finer resolution data such as downscaled soil moisture data sets (Garcia-Cardona et al., 2022; Xia et al., 2022) as model inputs, and strategically selected local field samples representing within-site variability (Xia, Sanderman, et al., 2024) for improved model calibration and validation.

5. Conclusions

The RCTM system is the first effort to combine RS-driven LUE model outputs with a process-based soil model for the estimation of C dynamics and SOC stocks in rangeland systems. There is a potential to apply the system to estimate rangeland productivity and soil C dynamics for across the US and other regions of the world, after the system is calibrated and validated with data sets representing the application domain. The RCTM system offers several key advantages. First, it is applicable in situations where rangeland management data sets, such as grazing intensity and duration, are unavailable. Second, RCTM can estimate long-term (20 years or more) rangeland C dynamics influenced by management and climate conditions. Furthermore, its flexible parameterization procedure allows for continuous model refinement as new flux tower and SOC data become available. Lastly, RCTM has a good potential in scalability, as it can be applied across different temporal scales and for both local and regional extents, while maintaining a relatively high spatial resolution (30 m) that is relevant to management. The regional estimates of rangeland productivity and SOC sequestration trends obtained from this work (e.g., increase in GPP and SOC tied to climate pattern) can be used to inform policy making and are suited to improve large-scale rangeland C monitoring efforts. At the same time, it will also be possible to apply RCTM at the site level (e.g., for individual operations) to track outcomes of management shifts, after parameterizing and verifying the system using targeted local data sets. High-resolution, quality-controlled RS data sets and field observations capturing management effects on rangeland dynamics are essential to support the continuous improvement of RCTM and other RS-driven process-based modeling systems for rangeland C monitoring.

Data Availability Statement

The codes used to develop the Rangeland Carbon Tracking and Monitoring system in the study are made publicly available at Xia, Mullen, et al. (2024) via <https://doi.org/10.5281/zenodo.14510807>.

Acknowledgments

This research was supported by Conscience Bay Research, Woodwell Fund for Climate Solutions, Mighty Arrow Family Foundation, and J.M. Kaplan Fund. The authors extend their sincere gratitude to AmeriFlux and NEON network PIs including Dr. Kimberly Novick, Dr. David Durden, Dr. Chris Florian, Dr. Cove Sturtevant, Dr. Stefan Metzger, Dr. David Bowling, Dr. Dennis Baldocchi, Dr. Camilo Rey-Sanchez, Dr. Sonia Wharton, Dr. Thomas Kolb, Dr. Sabina Dore, Dr. Dean Anderson, Dr. Elise Pendall, Dr. Mike Goulden, Dr. Roser Matamala, and Ross Bryant, for maintaining the sites and providing flux tower measurements. AmeriFlux is funded by the U.S. Department of Energy's Office of Science. Additional funding for a number of AmeriFlux sites in Arizona, New Mexico and Idaho comes from the U.S. Department of Agriculture's Long-term Agroecosystem Network. The National Ecological Observatory Network is a program sponsored by the National Science Foundation and operated under cooperative agreement by Battelle. The authors are also deeply grateful for the feedback and suggestions provided by Dr. Francesca Cotrufo for this project. The editor and three anonymous reviewers provided valuable comments and edits that helped improve this manuscript.

References

- Abdalla, M., Saunders, M., Hastings, A., Williams, M., Smith, P., Osborne, B., et al. (2013). Simulating the impacts of land use in Northwest Europe on Net Ecosystem Exchange (NEE): The role of arable ecosystems, grasslands and forest plantations in climate change mitigation. *Science of The Total Environment*, 465, 325–336. <https://doi.org/10.1016/j.scitotenv.2012.12.030>
- Ali, I., Cawkwell, F., Dwyer, E., Barrett, B., & Green, S. (2016). Satellite remote sensing of grasslands: From observation to management. *Journal of Plant Ecology*, 9(6), 649–671. <https://doi.org/10.1093/jpe/rtw005>
- Arndt, K. A., Campbell, E. E., Dorich, C. D., Grandy, A. S., Griffin, T. S., Ingraham, P., et al. (2022). Initial soil conditions outweigh management in a cool-season dairy farm's carbon sequestration potential. *Science of the Total Environment*, 809, e152195. <https://doi.org/10.1016/j.scitotenv.2021.152195>
- Badgley, G., Anderegg, L. D. L., Berry, J. A., & Field, C. B. (2019). Terrestrial gross primary production: Using NIR_v to scale from site to globe. *Global Change Biology*, 25(11), 3731–3740. <https://doi.org/10.1111/gcb.14729>
- Biederman, J. A., Scott, R. L., Bell, T. W., Bowling, D. R., Dore, S., Garatuza-Payan, J., et al. (2017). CO₂ exchange and evapotranspiration across dryland ecosystems of southwestern North America. *Global Change Biology*, 23(10), 4204–4221. <https://doi.org/10.1111/gcb.13686>
- Blanco-Canqui, H., & Lal, R. (2004). Mechanisms of carbon sequestration in soil aggregates. *Critical Reviews in Plant Sciences*, 23(6), 481–504. <https://doi.org/10.1080/0735268049086842>
- Bond-Lamberty, B., Christianson, D. S., Malhotra, A., Pennington, S. C., Sihi, D., AghaKouchak, A., et al. (2020). COSORE: A community database for continuous soil respiration and other soil-atmosphere greenhouse gas flux data. *Global Change Biology*, 26(12), 7268–7283. <https://doi.org/10.1111/gcb.15353>
- Booker, K., Huntsinger, L., Bartolome, J. W., Sayre, N. F., & Stewart, W. (2013). What can ecological science tell us about opportunities for carbon sequestration on arid rangelands in the United States? *Global Environmental Change*, 23(1), 240–251. <https://doi.org/10.1016/j.gloenvcha.2012.10.001>
- Bronaugh, D., Schoeneberg, A., & Zeman, L. (2023). Package 'zyp'. Retrieved from <https://cran.r-project.org/web/packages/zyp/zyp.pdf>
- Brown, T. B., Hultine, K. R., Steltzer, H., Denny, E. G., Denslow, M. W., Granados, J., et al. (2016). Using phenocams to monitor our changing earth: Toward a global phenocam network. *Frontiers in Ecology and the Environment*, 14(2), 84–93. <https://doi.org/10.1002/fee.1222>
- Browning, D. M., Snyder, K. A., & Herrick, J. E. (2019). Plant phenology: Taking the pulse of rangelands. *Rangelands*, 41(3), 129–134. <https://doi.org/10.1016/j.rala.2019.02.001>
- Cao, R., Chen, Y., Shen, M., Chen, J., Zhou, J., Wang, C., & Yang, W. (2018). A simple method to improve the quality of NDVI time-series data by integrating spatiotemporal information with the Savitzky-Golay filter. *Remote Sensing of Environment*, 217, 244–257. <https://doi.org/10.1016/j.rse.2018.08.022>
- Chang, X., Bao, X., Wang, S., Wilkes, A., Erdenetsetseg, B., Baival, B., et al. (2015). Simulating effects of grazing on soil organic carbon stocks in Mongolian grasslands. *Agriculture, Ecosystems & Environment*, 212, 278–284. <https://doi.org/10.1016/j.agee.2015.07.014>

- Chen, J., Chen, J., Liao, A., Cao, X., Chen, L., Chen, X., et al. (2015). Global land cover mapping at 30 m resolution: A POK-based operational approach. *ISPRS Journal of Photogrammetry and Remote Sensing*, 103, 7–27. <https://doi.org/10.1016/j.isprsjprs.2014.09.002>
- Chu, H., Christianson, D. S., Cheah, Y. W., Pastorello, G., O'Brien, F., Geden, J., et al. (2023). AmeriFlux BASE data pipeline to support network growth and data sharing. *Scientific Data*, 10(1), e614. <https://doi.org/10.1038/s41597-023-02531-2>
- Chu, H., Luo, X., Ouyang, Z., Chan, W. S., Dengel, S., Biraud, S. C., et al. (2021). Representativeness of eddy-covariance flux footprints for areas surrounding AmeriFlux sites. *Agricultural and Forest Meteorology*, 301–302, 108350. <https://doi.org/10.1016/j.agrformet.2021.108350>
- Coleman, K., & Jenkinson, D. S. (1996). RothC-26.3-A Model for the turnover of carbon in soil. In D. S. Powlson, P. Smith, & J. U. Smith (Eds.), *Evaluation of soil organic matter models: Using existing long-term datasets* (pp. 237–246). Springer. https://doi.org/10.1007/978-3-642-61094-3_17
- Conant, R. T., Cerri, C. E. P., Osborne, B. B., & Paustian, K. (2017). Grassland management impacts on soil carbon stocks: A new synthesis: A. *Ecological Applications*, 27(2), 662–668. <https://doi.org/10.1002/eap.1473>
- Cooter, E. J., Bash, J. O., Benson, V., & Ran, L. (2012). Linking agricultural crop management and air quality models for regional to national-scale nitrogen assessments. *Biogeosciences*, 9(10), 4023–4035. <https://doi.org/10.5194/bg-9-4023-2012>
- Delgado-Baquerizo, M., Eldridge, D. J., Maestre, F. T., Karunaratne, S. B., Trivedi, P., Reich, P. B., & Singh, B. K. (2017). Climate legacies drive global soil carbon stocks in terrestrial ecosystems. *Science Advances*, 3(4), e1602008. <https://doi.org/10.1126/sciadv.1602008>
- de Oliveira, D. C., Maia, S. M. F., Freitas, R. D. C. A., & Cerri, C. E. P. (2022). Changes in soil carbon and soil carbon sequestration potential under different types of pasture management in Brazil. *Regional Environmental Change*, 22(3), e87. <https://doi.org/10.1007/s10113-022-01945-9>
- Derner, J. D., Augustine, D. J., & Frank, D. A. (2019). Does grazing matter for soil organic carbon sequestration in the western North American Great Plains? *Ecosystems*, 22(5), 1088–1094. <https://doi.org/10.1007/s10021-018-0324-3>
- Derner, J. D., & Schuman, G. E. (2007). Carbon sequestration and rangelands: A synthesis of land management and precipitation effects. *Journal of Soil and Water Conservation*, 62(2), 77–85.
- Desai, A. R., Richardson, A. D., Moffat, A. M., Kattge, J., Hollinger, D. Y., Barr, A., et al. (2008). Cross-site evaluation of eddy covariance GPP and RE decomposition techniques. *Agricultural and Forest Meteorology*, 148(6–7), 821–838. <https://doi.org/10.1016/j.agrformet.2007.11.012>
- Endsley, A. K., Kimball, J. S., Reichle, R. H., & Watts, J. D. (2020). Satellite monitoring of global surface soil organic carbon dynamics using the SMAP Level 4 carbon product. *Journal of Geophysical Research: Biogeosciences*, 125(12), e2020JG006100. <https://doi.org/10.1029/2020JG006100>
- Fargione, J. E., Boucher, T., Bridgman, S. D., Conant, R. T., Bassett, S., Cook-Patton, S. C., et al. (2018). Natural climate solutions for the United States. *Science Advances*, 4(11), eaat1869. <https://doi.org/10.1126/sciadv.aat1869>
- Feldman, A. F., Reed, S., Amaral, C., Babst-Kostecka, A., Babst, F., Biederman, J., et al. (2024). Adaptation and response in drylands (ARID): Community insights for scoping a NASA terrestrial ecology field campaign in drylands. *Earth's Future*, 12(9), e2024EF004811. <https://doi.org/10.1029/2024EF004811>
- Forkel, M., Carvalhais, N., Schaphoff, S., Bloh, W. V., Migliavacca, M., Thurner, M., & Thonicke, K. (2014). Identifying environmental controls on vegetation greenness phenology through model-data integration. *Biogeosciences*, 11(23), 7025–7050. <https://doi.org/10.5194/bg-11-7025-2014>
- Fuhlendorf, S. D., Briske, D. D., & Smeins, F. E. (2000). Herbaceous vegetation change in variable rangeland environments: The relative contribution of grazing and climatic variability. *Applied Vegetation Science*, 4(2), 177–188. <https://doi.org/10.1111/j.1654-109x.2001.tb00486.x>
- Gao, F., Masek, J., Schwaller, M., & Hall, F. (2006). On the blending of the landsat and MODIS surface reflectance: Predicting daily landsat surface reflectance. *IEEE Transactions on Geoscience and Remote Sensing*, 44(8), 2207–2218. <https://doi.org/10.1109/TGRS.2006.872081>
- Gao, J., Liang, T., Liu, J., Yin, J., Ge, J., Hou, M., et al. (2020). Potential of hyperspectral data and machine learning algorithms to estimate the forage carbon-nitrogen ratio in an alpine grassland ecosystem of the Tibetan Plateau. *ISPRS Journal of Photogrammetry and Remote Sensing*, 163, 362–374. <https://doi.org/10.1016/j.isprsjprs.2020.03.017>
- García-Cardona, J., Ortega, A., & Rodríguez-Alvarez, N. (2022). Downscaling SMAP soil moisture with Ecstress products using a graph-based interpolation method. *International Geoscience and Remote Sensing Symposium (IGARSS)*, 7, 6169–6172. <https://doi.org/10.1109/IGARSS46834.2022.9883945>
- Gelman, A., & Rubin, D. B. (1989). Inference from iterative simulation using multiple sequences. *Statistics*, 10(1), 409–435.
- Golodets, C., Sternberg, M., Kigel, J., Boeken, B., Henkin, Z., Seligman, N. G., & Ungar, E. D. (2013). From desert to Mediterranean rangelands: Will increasing drought and inter-annual rainfall variability affect herbaceous annual primary productivity? *Climatic Change*, 119(3–4), 785–798. <https://doi.org/10.1007/s10584-013-0758-8>
- Gorelick, N., Hancher, M., Dixon, M., Ilyushchenko, S., Thau, D., & Moore, R. (2017). Google Earth Engine: Planetary-scale geospatial analysis for everyone. *Remote Sensing of Environment*, 202, 18–27. <https://doi.org/10.1016/j.rse.2017.06.031>
- Gu, Y., Wylie, B. K., Howard, D. M., Phuyal, K. P., & Ji, L. (2013). NDVI saturation adjustment: A new approach for improving cropland performance estimates in the Greater Platte River Basin, USA. *Ecological Indicators*, 30, 1–6. <https://doi.org/10.1016/j.ecolind.2013.01.041>
- Guerschman, J. P., Paruelo, J. M., Di Bella, C., Giallorenzi, M. C., & Pacin, F. (2003). Land cover classification in the Argentine Pampas using multi-temporal Landsat TM data. *International Journal of Remote Sensing*, 24(17), 3381–3402. <https://doi.org/10.1080/0143116021000021288>
- Hall, D. K., Riggs, G. A., Salomonson, V. V., DiGirolamo, N. E., & Bayr, K. J. (2002). MODIS snow-cover products. *Remote Sensing of Environment*, 83(1–2), 181–194. [https://doi.org/10.1016/S0034-4257\(02\)00095-0](https://doi.org/10.1016/S0034-4257(02)00095-0)
- Hao, Y., & He, Z. (2019). Effects of grazing patterns on grassland biomass and soil environments in China: A meta-analysis. *PLoS One*, 14(4), e0215223. <https://doi.org/10.1371/journal.pone.0215223>
- Hartig, F., Minunno, F., Paul, S., Cameron, D., Tankred, O., & Maximilian, P. (2023). BayesianTools: General-purpose MCMC and SMC samplers and tools for Bayesian statistics. Retrieved from <https://cran.r-project.org/web/packages/BayesianTools/index.html>
- Hartigan, T., Hartigan, D. C., Maechler, M. M., Maechler, A. M., Ringach, D., Gpl, L., & Date, R. C. (2019). Package “tsoutliers”: Detection of outliers in time series. Retrieved from <http://r.meteo.uni.wroc.pl/web/packages/tsoutliers/tsoutliers.pdf>
- Hartman, M. D., Merchant, E. R., Parton, W. J., Gutmann, M. P., Lutz, S. M., & Williams, S. A. (2011). Impact of historical land-use changes on greenhouse gas exchange in the US Great Plains, 1883–2003. *Ecological Applications*, 21(4), 1105–1119. <https://doi.org/10.1890/10-0036.1>
- Hassink, J. (1997). The capacity of soils to preserve organic C and N by their association with clay and silt particles. *Plant and Soil*, 191(1), 77–87. <https://doi.org/10.1023/A:1004213929699>
- He, M., Chen, S., Lian, X., Wang, X., Peñuelas, J., & Piao, S. (2022). Global spectrum of vegetation light-use efficiency. *Geophysical Research Letters*, 49(16), e2022GL099550. <https://doi.org/10.1029/2022GL099550>

- Heimsath, A. M., Furbish, D. J., & Dietrich, W. E. (2005). The illusion of diffusion: Field evidence for depth-dependent sediment transport. *Geology*, 33(12), 949–952. <https://doi.org/10.1130/G21868.1>
- Heuvelink, G. B. M., Angelini, M. E., Poggio, L., Bai, Z., Batjes, N. H., van den Bosch, R., et al. (2021). Machine learning in space and time for modelling soil organic carbon change. *European Journal of Soil Science*, 72(4), 1607–1623. <https://doi.org/10.1111/ejss.12998>
- Hill, M. J., Roxburgh, S. H., McKeon, G. M., Carter, J. O., & Barrett, D. J. (2006). Analysis of soil carbon outcomes from interaction between climate and grazing pressure in Australian rangelands using Range-ASSESS. *Environmental Modelling and Software*, 21(6), 779–801. <https://doi.org/10.1016/j.envsoft.2005.02.006>
- Hinckley, E. L. S., Bonan, G. B., Bowen, G. J., Colman, B. P., Duffy, P. A., Goodale, C. L., et al. (2016). The soil and plant biogeochemistry sampling design for the National Ecological Observatory Network. *Ecosphere*, 7(3), e01234. <https://doi.org/10.1002/ecs2.1234>
- Holechek, J. L., Geli, H. M. E., Cibils, A. F., & Sawalrah, M. N. (2020). Climate change, rangelands, and sustainability of ranching in the Western United States. *Sustainability*, 12(12), e4942. <https://doi.org/10.3390/su12124942>
- Homer, C., Dewitz, J., Fry, J., Coan, M., Hossain, N., Larson, C., et al. (2007). Completion of the 2001 National Land Cover Database for the conterminous United States. *Photogrammetric Engineering and Remote Sensing*, 73(4), 337–341.
- Homer, C. G., Dewitz, J. A., Yang, L., Jin, S., Danielson, P., Xian, G., et al. (2015). Completion of the 2011 National Land Cover Database for the conterminous United States-Representing a decade of land cover change information. *Photogrammetric Engineering and Remote Sensing*, 81(5), 345–354. <https://doi.org/10.14358/PERS.81.5.345>
- Hossain, M. L., & Li, J. (2021). Biomass partitioning of C3- and C4-dominated grasslands in response to climatic variability and climate extremes. *Environmental Research Letters*, 16(7), e074016. <https://doi.org/10.1088/1748-9326/ac027a>
- Huang, K., Zhang, Y., Tagesson, T., Brandt, M., Wang, L., Chen, N., et al. (2021). The confounding effect of snow cover on assessing spring phenology from space: A new look at trends on the Tibetan Plateau. *Science of the Total Environment*, 756, e144011. <https://doi.org/10.1016/j.scitotenv.2020.144011>
- Huete, A. R., & Jackson, R. D. (1988). Soil and atmosphere influences on the spectra of partial canopies. *Remote Sensing of Environment*, 25(1), 89–105. [https://doi.org/10.1016/0034-4257\(88\)90043-0](https://doi.org/10.1016/0034-4257(88)90043-0)
- Hui, D., & Jackson, R. B. (2006). Geographical and interannual variability in biomass partitioning in grassland ecosystems: A synthesis of field data. *New Phytologist*, 169(1), 85–93. <https://doi.org/10.1111/j.1469-8137.2005.01569.x>
- Huys, R., Poirier, V., Bourget, M. Y., Roumet, C., Hättenschwiler, S., Fromin, N., et al. (2022). Plant litter chemistry controls coarse-textured soil carbon dynamics. *Journal of Ecology*, 110(12), 2911–2928. <https://doi.org/10.1111/1365-2745.13997>
- Izaurrealde, R. C., Thomson, A. M., Morgan, J. A., Fay, P. A., Polley, H. W., & Hatfield, J. L. (2011). Climate impacts on agriculture: Implications for forage and rangeland production. *Agronomy Journal*, 103(2), 371–381. <https://doi.org/10.2134/agronj2010.0304>
- Jebbari, A., Álvaro-Fuentes, J., Pardo, G., Almagro, M., & del Prado, A. (2021). Estimating soil organic carbon changes in managed temperate moist grasslands with RothC. *PLoS One*, 16(8), e0256219. <https://doi.org/10.1371/journal.pone.0256219>
- Jin, H., Bao, G., Chen, J., Chopping, M., Jin, E., Mandakh, U., et al. (2020). Modifying the maximal light-use efficiency for enhancing predictions of vegetation net primary productivity on the Mongolian Plateau. *International Journal of Remote Sensing*, 41(10), 3740–3760. <https://doi.org/10.1080/01431161.2019.1707902>
- Jones, M. O., Allred, B. W., Naugle, D. E., Maestas, J. D., Donnelly, P., Metz, L. J., et al. (2018). Innovation in rangeland monitoring: Annual, 30 m, plant functional type percent cover maps for U.S. rangelands, 1984–2017. *Ecosphere*, 9, e02430. <https://doi.org/10.1002/ecs2.2430>
- Keller, M., Schimel, D. S., Hargrove, W. W., & Hoffman, F. M. (2008). A continental strategy for the National Ecological Observatory Network. *Frontiers in Ecology and the Environment*, 6(5), 282–284. [https://doi.org/10.1890/1540-9295\(2008\)6\[282:ACSFTN\]2.0.CO;2](https://doi.org/10.1890/1540-9295(2008)6[282:ACSFTN]2.0.CO;2)
- Kelley, D. (2013). Package “oce”: Analysis of oceanographic data. Retrieved from <https://cran.r-project.org/web/packages/oce/oce.pdf>
- Kelly, R. H., Parton, W. J., Hartman, M. D., Stretch, L. K., Ojima, D. S., & Schimel, D. S. (2000). Intra-annual and interannual variability of ecosystem processes in shortgrass steppe. *Journal of Geophysical Research*, 105(D15), 20093–20100. <https://doi.org/10.1029/2000JD900259>
- Kovalsky, V., & Roy, D. P. (2013). The global availability of Landsat 5 TM and Landsat 7 ETM+ land surface observations and implications for global 30m Landsat data product generation. *Remote Sensing of Environment*, 130, 280–293. <https://doi.org/10.1016/j.rse.2012.12.003>
- Krause, A., Papastefanou, P., Gregor, K., Layritz, L. S., Zang, C. S., Buras, A., et al. (2022). Quantifying the impacts of land cover change on gross primary productivity globally. *Scientific Reports*, 12(1), e18398. <https://doi.org/10.1038/s41598-022-23120-0>
- Lange, M., Feilhauer, H., Kühn, I., & Doktor, D. (2022). Mapping land-use intensity of grasslands in Germany with machine learning and Sentinel-2 time series. *Remote Sensing of Environment*, 277, e112888. <https://doi.org/10.1016/j.rse.2022.112888>
- Li, C., Froliking, S., & Harriss, R. (1994). Modeling carbon biogeochemistry in agricultural soils. *Global Biogeochemical Cycles*, 8(3), 237–254. <https://doi.org/10.1029/94GB00767>
- Li, C., Salas, W., Zhang, R., Krauter, C., Rotz, A., & Mitloehner, F. (2012). Manure-DNDC: A biogeochemical process model for quantifying greenhouse gas and ammonia emissions from livestock manure systems. *Nutrient Cycling in Agroecosystems*, 93(2), 163–200. <https://doi.org/10.1007/s10705-012-9507-z>
- Li, L., Zhang, Y., Liu, L., Wu, J., Li, S., Zhang, H., et al. (2018). Current challenges in distinguishing climatic and anthropogenic contributions to alpine grassland variation on the Tibetan Plateau. *Ecology and Evolution*, 8(11), 5949–5963. <https://doi.org/10.1002/ece3.4099>
- Liu, H., Jin, Y., Roche, L. M., O'Geen, A. T., & Dahlgren, R. A. (2021). Understanding spatial variability of forage production in California grasslands: Delineating climate, topography and soil controls. *Environmental Research Letters*, 16(1), e014043. <https://doi.org/10.1088/1748-9326/abc64d>
- Long, X., Guan, H., Sinclair, R., Batelaan, O., Facelli, J. M., Andrew, R. L., & Bestland, E. (2019). Response of vegetation cover to climate variability in protected and grazed arid rangelands of South Australia. *Journal of Arid Environments*, 161, 64–71. <https://doi.org/10.1016/j.jaridenv.2018.10.001>
- Maher, A. T., Ashwell, N. E. Q., MacZko, K. A., Taylor, D. T., Tanaka, J. A., & Reeves, M. C. (2021). An economic valuation of federal and private grazing land ecosystem services supported by beef cattle ranching in the United States. *Translational Animal Science*, 5(3), 1–15. <https://doi.org/10.1093/tas/txab054>
- Mao, H. R., Cotrufo, M. F., Hart, S. C., Sullivan, B. W., Zhu, X., Zhang, J., et al. (2024). Dual role of silt and clay in the formation and accrual of stabilized soil organic carbon. *Soil Biology and Biochemistry*, 192, e109390. <https://doi.org/10.1016/j.soilbio.2024.109390>
- McSherry, M. E., & Ritchie, M. E. (2013). Effects of grazing on grassland soil carbon: A global review. *Global Change Biology*, 19(5), 1347–1357. <https://doi.org/10.1111/gcb.12144>
- Milne, R. M., & Haynes, R. J. (2004). Soil organic matter, microbial properties, and aggregate stability under annual and perennial pastures. *Biology and Fertility of Soils*, 39(3), 172–178. <https://doi.org/10.1007/s00374-003-0698-y>
- Moll-Mielewicz, J., Keel, S. G., & Gubler, A. (2023). Organic carbon contents of mineral grassland soils in Switzerland over the last 30 years. *Agriculture, Ecosystems and Environment*, 342, e108258. <https://doi.org/10.1016/j.agee.2022.108258>

- Nave, L. E., Bowman, M., Gallo, A., Hatten, J. A., Heckman, K. A., Matosziuk, L., et al. (2021). Patterns and predictors of soil organic carbon storage across a continental-scale network. *Biogeochemistry*, 156(1), 75–96. <https://doi.org/10.1007/s10533-020-00745-9>
- Nie, W., Kumar, S. V., Bindlish, R., Liu, P. W., & Wang, S. (2022). Remote sensing-based vegetation and soil moisture constraints reduce irrigation estimation uncertainty. *Environmental Research Letters*, 17(8), e084010. <https://doi.org/10.1088/1748-9326/ac7ed8>
- Novick, K. A., Biederman, J. A., Desai, A. R., Litvak, M. E., Moore, D. J. P., Scott, R. L., & Torn, M. S. (2018). The AmeriFlux network: A coalition of the willing. *Agricultural and Forest Meteorology*, 249, 444–456. <https://doi.org/10.1016/j.agrformet.2017.10.009>
- Numata, I., Roberts, D. A., Chadwick, O. A., Schimel, J., Sampaio, F. R., Leonidas, F. C., & Soares, J. V. (2007). Characterization of pasture biophysical properties and the impact of grazing intensity using remotely sensed data. *Remote Sensing of Environment*, 109(3), 314–327. <https://doi.org/10.1016/j.rse.2007.01.013>
- Oliphant, A. J. (2012). Terrestrial ecosystem-atmosphere exchange of CO₂, water and energy from FLUXNET: Review and meta-analysis of a global in-situ observatory. *Geography Compass*, 6(12), 689–705. <https://doi.org/10.1111/gec3.12009>
- Olson, D. M., Dinerstein, E., Wikramanayake, E. D., Burgess, N. D., Powell, G. V. N., Underwood, E. C., et al. (2001). Terrestrial ecoregions of the world: A new map of life on Earth. *BioScience*, 51(11), 933–938. [https://doi.org/10.1641/0006-3568\(2001\)051\[0933:teotwa\]2.0.co;2](https://doi.org/10.1641/0006-3568(2001)051[0933:teotwa]2.0.co;2)
- Otunga, C., Odindi, J., Mutanga, O., & Adjorlolo, C. (2019). Evaluating the potential of the red edge channel for C3 (Festuca spp.) grass discrimination using Sentinel-2 and Rapid Eye satellite image data. *Geocarto International*, 34(10), 1123–1143. <https://doi.org/10.1080/10106049.2018.1474274>
- Parton, W. J., Hartman, M., Ojima, D., & Schimel, D. (1998). DAYCENT and its land surface submodel: Description and testing. *Global and Planetary Change*, 19(1–4), 35–48. [https://doi.org/10.1016/S0921-8181\(98\)00040-X](https://doi.org/10.1016/S0921-8181(98)00040-X)
- Paudel, K. P., & Andersen, P. (2010). Assessing rangeland degradation using multi temporal satellite images and grazing pressure surface model in Upper Mustang, Trans Himalaya, Nepal. *Remote Sensing of Environment*, 114(8), 1845–1855. <https://doi.org/10.1016/j.rse.2010.03.011>
- Peng, D., Zhang, B., & Liu, L. (2012). Comparing spatiotemporal patterns in Eurasian FPAR derived from two NDVI-based methods. *International Journal of Digital Earth*, 5(4), 283–298. <https://doi.org/10.1080/17538947.2011.598193>
- Pepper, D. A., Del Grosso, S. J., McMurtrie, R. E., & Parton, W. J. (2005). Simulated carbon sink response of shortgrass steppe, tallgrass prairie and forest ecosystems to rising [CO₂], temperature and nitrogen input. *Global Biogeochemical Cycles*, 19(1), 1–20. <https://doi.org/10.1029/2004GB002226>
- Phukubye, K., Mutema, M., Buthelezi, N., Muchaonyerwa, P., Cerri, C., & Chaplot, V. (2022). On the impact of grassland management on soil carbon stocks: A worldwide meta-analysis. *Geoderma Regional*, 28, e00479. <https://doi.org/10.1016/j.geodrs.2021.e00479>
- Qi, Y., Wei, W., Chen, C., & Chen, L. (2019). Plant root-shoot biomass allocation over diverse biomes: A global synthesis. *Global Ecology and Conservation*, 18, e00606. <https://doi.org/10.1016/j.gecco.2019.e00606>
- Ramcharan, A., Hengl, T., Nauman, T., Brungard, C., Waltman, S., Willis, S., & Thompson, J. (2018). Soil property and class maps of the conterminous United States at 100-meter spatial resolution. *Soil Science Society of America Journal*, 82(1), 186–201. <https://doi.org/10.2136/sssaj2017.04.0122>
- R Core Team. (2023). R: A language and environment for Statistical Computing [Software]. *R Foundation*. Retrieved from <https://www.r-project.org/>
- Reeves, M. C., & Mitchell, J. E. (2011). Extent of coterminous US rangelands: Quantifying implications of differing agency perspectives. *Rangeland Ecology and Management*, 64(6), 585–597. <https://doi.org/10.2111/REM-D-11-00035.1>
- Reinermann, S., Asam, S., & Kuenzer, C. (2020). Remote sensing of grassland production and management-A review. *Remote Sensing*, 12(12), e1949. <https://doi.org/10.3390/rs12121949>
- Rolfe, J., Star, M., & Curcio, A. (2021). Can extension programs improve grazing management in rangelands: A case study in Australia's Great Barrier Reef catchments. *Rangeland Journal*, 42(6), 447–459. <https://doi.org/10.1071/RJ20098>
- Rossum, G. V., & Drake, F. L. (1995). Python tutorial. Retrieved from <http://www.python.org/doc/ref/>
- Roy, D. P., Wulder, M. A., Loveland, T. R., Woodcock, C. E., Allen, R. G., Anderson, M. C., et al. (2014). Landsat-8: Science and product vision for terrestrial global change research. *Remote Sensing of Environment*, 145, 154–172. <https://doi.org/10.1016/j.rse.2014.02.001>
- Sanderman, J., & Amundson, R. (2008). A comparative study of dissolved organic carbon transport and stabilization in California forest and grassland soils. *Biogeochemistry*, 89(3), 309–327. <https://doi.org/10.1007/s10533-008-9221-8>
- Sanderman, J., Hengl, T., & Fiske, G. J. (2017). Soil carbon debt of 12,000 years of human land use. *Proceedings of the National Academy of Sciences of the United States of America*, 114(36), 9575–9580. <https://doi.org/10.1073/pnas.1706103114>
- Sanderson, J. S., Beutler, C., Brown, J. R., Burke, I., Chapman, T., Conant, R. T., et al. (2020). Cattle, conservation, and carbon in the western Great Plains. *Journal of Soil and Water Conservation*, 75(1), 5A–12A. <https://doi.org/10.2489/JSWC.75.1.5A>
- Sándor, R., Barcza, Z., Hidy, D., Lellei-Kovács, E., Ma, S., & Bellocchi, G. (2016). Modelling of grassland fluxes in Europe: Evaluation of two biogeochemical models. *Agriculture, Ecosystems and Environment*, 215, 1–19. <https://doi.org/10.1016/j.agee.2015.09.001>
- Schaa, C., & Wang, Z. (2015). MODIS/Terra and Aqua Nadir BRDF-Adjusted Reflectance Daily L3 Global 500 m SIN Grid V006. <https://doi.org/10.5067/MODIS/MCD43A4.061>
- Schenk, H. J., & Jackson, R. B. (2002). Rooting depths, lateral root spreads and below-ground/above-ground allometries of plants in water-limited ecosystems. *Journal of Ecology*, 90(3), 480–494. <https://doi.org/10.1046/j.1365-2745.2002.00682.x>
- Schmelzer, L., Perryman, B., Bruce, B., Schultz, B., McAdoo, K., McCuin, G., et al. (2014). Case study: Reducing cheatgrass (*Bromus tectorum* L.) fuel loads using fall cattle grazing. *Professional Animal Scientist*, 30(2), 270–278. [https://doi.org/10.15232/S1080-7446\(15\)30112-1](https://doi.org/10.15232/S1080-7446(15)30112-1)
- Scott, R. L., Johnston, M. R., Knowles, J. F., MacBean, N., Mahmud, K., Roby, M. C., & Dannenberg, M. P. (2023). Interannual variability of spring and summer monsoon growing season carbon exchange at a semiarid savanna over nearly two decades. *Agricultural and Forest Meteorology*, 339, e109584. <https://doi.org/10.1016/j.agrformet.2023.109584>
- Shibia, M. G., Röder, A., Fava, F. P., Stellmes, M., & Hill, J. (2022). Integrating satellite images and topographic data for mapping seasonal grazing management units in pastoral landscapes of eastern Africa. *Journal of Arid Environments*, 197, e104661. <https://doi.org/10.1016/j.jaridenv.2021.104661>
- Sibanda, M., Mutanga, O., & Rouget, M. (2016). Comparing the spectral settings of the new generation broad and narrow band sensors in estimating biomass of native grasses grown under different management practices. *GIScience & Remote Sensing*, 53(5), 614–633. <https://doi.org/10.1080/15481603.2016.1221576>
- Silverman, N. L., Allred, B. W., Donnelly, J. P., Chapman, T. B., Maestas, J. D., Wheaton, J. M., et al. (2019). Low-tech riparian and wet meadow restoration increases vegetation productivity and resilience across semiarid rangelands. *Restoration Ecology*, 27(2), 269–278. <https://doi.org/10.1111/rec.12869>
- Smet, M., & Ward, D. (2005). A comparison of the effects of different rangeland management systems on plant species composition, diversity and vegetation structure in a semi-arid savanna. *African Journal of Range and Forage Science*, 22(1), 59–71. <https://doi.org/10.2989/10220110509485862>

- Smith, S. W., Vandenbergh, C., Hastings, A., Johnson, D., Pakeman, R. J., van der Wal, R., & Woodin, S. J. (2014). Optimizing carbon storage within a spatially heterogeneous upland grassland through sheep grazing management. *Ecosystems*, 17(3), 418–429. <https://doi.org/10.1007/s10021-013-9731-7>
- Stoy, P. C., Cook, A. A., Dore, J. E., Kljun, N., Kleindl, W., Jack Brookshire, E. N., & Gerken, T. (2021). Methane efflux from an American bison herd. *Biogeosciences*, 18(3), 961–975. <https://doi.org/10.5194/bg-18-961-2021>
- Su, Y., Dong, K., Wang, C., & Liu, X. (2022). Grazing promoted plant litter decomposition and nutrient release: A meta-analysis. *Agriculture, Ecosystems and Environment*, 337, e108051. <https://doi.org/10.1016/j.agee.2022.108051>
- Sulman, B. N., Roman, D. T., Scanlon, T. M., Wang, L., & Novick, K. A. (2016). Comparing methods for partitioning a decade of carbon dioxide and water vapor fluxes in a temperate forest. *Agricultural and Forest Meteorology*, 226–227, 229–245. <https://doi.org/10.1016/j.agrformet.2016.06.002>
- Ter Braak, C. J. F., & Vrugt, J. A. (2008). Differential evolution Markov chain with snooker updater and fewer chains. *Statistics and Computing*, 18(4), 435–446. <https://doi.org/10.1007/s11222-008-9104-9>
- Thornton, M. M., Thornton, P. E., Wei, Y., Mayer, B. W., Cook, R. B., & Vose, R. S. (2022). *Daymet: Monthly climate summaries on a 1-km grid for North America, version 4 R1*. Oak Ridge National Laboratory. <https://doi.org/10.3334/ORNLDAAAC/2131>
- Tramontana, G., Migliavacca, M., Jung, M., Reichstein, M., Keenan, T. F., Camps-Valls, G., et al. (2020). Partitioning net carbon dioxide fluxes into photosynthesis and respiration using neural networks. *Global Change Biology*, 26(9), 5235–5253. <https://doi.org/10.1111/gcb.15203>
- Tucker, C. J. (1979). Red and photographic infrared linear combinations for monitoring vegetation. *Remote Sensing of Environment*, 8(2), 127–150. [https://doi.org/10.1016/0034-4257\(79\)90013-0](https://doi.org/10.1016/0034-4257(79)90013-0)
- Turner, D. P., Ollinger, S. V., & Kimball, J. S. (2004). Integrating remote sensing and ecosystem process models for landscape- to regional-scale analysis of the carbon cycle. *BioScience*, 54(6), 573–584. [https://doi.org/10.1641/0006-3568\(2004\)054\[0573:IRSAEPJ2.0.CO;2](https://doi.org/10.1641/0006-3568(2004)054[0573:IRSAEPJ2.0.CO;2)
- Twine, T. E., & Kucharik, C. J. (2008). Evaluating a terrestrial ecosystem model with satellite information of greenness. *Journal of Geophysical Research*, 113(3), e2007JG000599. <https://doi.org/10.1029/2007JG000599>
- United States Geological Survey. (2019). Phase 2 gap-fill algorithm: SLC-off gap-filled products gap-fill algorithm methodology. Retrieved from <https://www.usgs.gov/media/files/landsat-7-slc-gap-filled-products-phase-two-methodology>
- van Zyl, J. J. (2001). The shuttle radar topography mission (SRTM): A breakthrough in remote sensing of topography. *Acta Astronautica*, 48(5–12), 559–565. [https://doi.org/10.1016/S0094-5765\(01\)00020-0](https://doi.org/10.1016/S0094-5765(01)00020-0)
- Wang, C., Zhang, W., Li, X., Hou, Y., & Wu, J. (2021). A global meta-analysis of the effects of plant diversity on biomass partitioning in grasslands. *Environmental Research Letters*, 16(6), e064083. <https://doi.org/10.1088/1748-9326/ac0747>
- Wang, C., Zhong, C., & Yang, Z. (2014). Assessing bioenergy-driven agricultural land use change and biomass quantities in the U.S. Midwest with MODIS time series. *Journal of Applied Remote Sensing*, 8(1), e085198. <https://doi.org/10.1117/1.jrs.8.085198>
- Wang, G., Mao, J., Fan, L., Ma, X., & Li, Y. (2022). Effects of climate and grazing on the soil organic carbon dynamics of the grasslands in Northern Xinjiang during the past twenty years. *Global Ecology and Conservation*, 34, e02039. <https://doi.org/10.1016/j.gecco.2022.e02039>
- Wang, J., Liu, J., Cao, M., Liu, Y., Yu, G., Li, G., et al. (2011). Modelling carbon fluxes of different forests by coupling a remote-sensing model with an ecosystem process model. *International Journal of Remote Sensing*, 32(21), 6539–6567. <https://doi.org/10.1080/01431161.2010.512933>
- Waterhouse, H., Aburto, F., Rees, G., Griffin-LaHue, D. E., Salls, W. B., Rippner, D. A., et al. (2023). Diversified vegetation types on rangelands promote multiple soil-based ecosystem services. *Land Degradation & Development*, 35(3), 1011–1028. <https://doi.org/10.1002/ldr.4967>
- Watts, J. D., Farina, M., Kimball, J. S., Schiferl, L. D., Liu, Z., Arndt, K. A., et al. (2023). Carbon uptake in Eurasian boreal forests dominates the high-latitude net ecosystem carbon budget. *Global Change Biology*, 29(7), 1870–1889. <https://doi.org/10.1111/gcb.16553>
- Watts, J. D., Kimball, J. S., Parmentier, F. J. W., Sachs, T., Rinne, J., Zona, D., et al. (2024). A satellite data driven biophysical modeling approach for estimating northern peatland and tundra CO₂ and CH₄ fluxes. *Biogeosciences*, 11(7), 1961–1980. <https://doi.org/10.5194/bg-11-1961-2014>
- Watts, J. D., Powell, S. L., Lawrence, R. L., & Hilker, T. (2011). Improved classification of conservation tillage adoption using high temporal and synthetic satellite imagery. *Remote Sensing of Environment*, 115(1), 66–75. <https://doi.org/10.1016/j.rse.2010.08.005>
- Williams, D. L., Goward, S., & Arvidson, T. (2006). Landsat: Yesterday, today, and tomorrow. *Photogrammetric Engineering and Remote Sensing*, 72(10), 1171–1178. <https://doi.org/10.14358/PERS.72.10.1171>
- Wilson, K. C., Rehmeier, R. L., Knight, G. L., Wiggam, S., Falke, J. A., Dalglish, H. J., et al. (2008). Comparing ecosystem goods and services provided by restored and native lands. *BioScience*, 58(9), 837–845. <https://doi.org/10.1641/b580909>
- Xia, Y., Ford, T. W., Wu, Y., Quiring, S. M., & Ek, M. B. (2015). Automated quality control of in situ soil moisture from the North American Soil Moisture Database using NLDAS-2 products. *Journal of Applied Meteorology and Climatology*, 54(6), 1267–1282. <https://doi.org/10.1175/JAMC-D-14-0275.1>
- Xia, Y., Mitchell, K., Ek, M., Sheffield, J., Cosgrove, B., Wood, E., et al. (2012). NLDAS Noah Land Surface Model L4 Hourly 0.125 x 0.125 degree V002. Retrieved from https://disc.gsfc.nasa.gov/datasets/NLDAS_NOAH0125_H_002/summary
- Xia, Y., Mullen, A., Rivard, C., Hernandez, H., Watts, J., Sanderman, J., & Machmuller, M. (2024). whrc/Rangeland-Carbon: v1.0.1 (v1.0.1) [Software]. Zenodo. <https://doi.org/10.5281/zenodo.11508223>
- Xia, Y., Sanderman, J., Watts, J. D., Machmuller, M. B., Ewing, S., & Rivard, C. (2024). Leveraging legacy data with targeted field sampling for low-cost mapping of soil organic carbon stocks on extensive rangeland properties. *Geoderma*, 448, e116952. <https://doi.org/10.1016/j.geoderma.2024.116952>
- Xia, Y., Watts, J. D., Machmuller, M. B., & Sanderman, J. (2022). Machine learning based estimation of field-scale daily, high resolution, multi-depth soil moisture for the Western and Midwestern United States. *PeerJ*, 10, e14275. <https://doi.org/10.7717/peerj.14275>
- Xu, B., Yang, X. C., Tao, W. G., Qin, Z. H., Liu, H. Q., Miao, J. M., & Bi, Y. Y. (2008). Modis-based remote sensing monitoring of grass production in China. *International Journal of Remote Sensing*, 29(17–18), 5313–5327. <https://doi.org/10.1080/01431160802036276>
- Yang, F., Weisberg, P. J., & Bristow, N. A. (2012). Landsat remote sensing approaches for monitoring long-term tree cover dynamics in semi-arid woodlands: Comparison of vegetation indices and spectral mixture analysis. *Remote Sensing of Environment*, 119, 62–71. <https://doi.org/10.1016/j.rse.2011.12.004>
- Yuan, W., Liu, S., Zhou, G., Zhou, G., Tieszen, L. L., Baldocchi, D., et al. (2007). Deriving a light use efficiency model from eddy covariance flux data for predicting daily gross primary production across biomes. *Agricultural and Forest Meteorology*, 143(3–4), 189–207. <https://doi.org/10.1016/j.agrformet.2006.12.001>
- Yue, S., Pilon, P., Phinney, B., & Cavadias, G. (2002). The influence of autocorrelation on the ability to detect trend in hydrological series. *Hydrological Processes*, 16(9), 1807–1829. <https://doi.org/10.1002/hyp.1095>
- Zhang, F., Chen, J. M., Chen, J., Gough, C. M., Martin, T. A., & Dragoni, D. (2012). Evaluating spatial and temporal patterns of MODIS GPP over the conterminous U.S. against flux measurements and a process model. *Remote Sensing of Environment*, 124, 717–729. <https://doi.org/10.1016/j.rse.2012.06.023>

- Zhang, L., Wylie, B., Loveland, T., Fosnight, E., Tieszen, L. L., Ji, L., & Gilmanov, T. (2007). Evaluation and comparison of gross primary production estimates for the Northern Great Plains grasslands. *Remote Sensing of Environment*, 106(2), 173–189. <https://doi.org/10.1016/j.rse.2006.08.012>
- Zhang, L. X., Zhou, D. C., Fan, J. W., & Hu, Z. M. (2015). Comparison of four light use efficiency models for estimating terrestrial gross primary production. *Ecological Modelling*, 300, 30–39. <https://doi.org/10.1016/j.ecolmodel.2015.01.001>
- Zhang, W., Zhang, F., Qi, J., & Hou, F. (2017). Modeling impacts of climate change and grazing effects on plant biomass and soil organic carbon in the Qinghai-Tibetan grasslands. *Biogeosciences*, 14(23), 5455–5470. <https://doi.org/10.5194/bg-14-5455-2017>
- Zhang, Y., Lavallee, J. M., Robertson, A. D., Even, R., Ogle, S. M., Paustian, K., & Cotrufo, M. F. (2021). Simulating measurable ecosystem carbon and nitrogen dynamics with the mechanistically defined MEMS 2.0 model. *Biogeosciences*, 18(10), 3147–3171. <https://doi.org/10.5194/bg-18-3147-2021>
- Zhang, Y., Tang, Y., Jiang, J., & Yang, Y. (2007). Characterizing the dynamics of soil organic carbon in grasslands on the Qinghai-Tibetan Plateau. *Science in China Series D: Earth Sciences*, 50(1), 113–120. <https://doi.org/10.1007/s11430-007-2032-2>
- Zhou, W., Guan, K., Peng, B., Tang, J., Jin, Z., Jiang, C., et al. (2021). Quantifying carbon budget, crop yields and their responses to environmental variability using the ecosys model for U.S. Midwestern agroecosystems. *Agricultural and Forest Meteorology*, 307, e108521. <https://doi.org/10.1016/j.agrformet.2021.108521>
- Zhu, X., & Liu, D. (2015). Improving forest aboveground biomass estimation using seasonal Landsat NDVI time-series. *ISPRS Journal of Photogrammetry and Remote Sensing*, 102, 222–231. <https://doi.org/10.1016/j.isprsjprs.2014.08.014>
- Zhu, X., Pei, Y., Zheng, Z., Dong, J., Zhang, Y., Wang, J., et al. (2018). Underestimates of grassland gross primary production in MODIS standard products. *Remote Sensing*, 10(11), e1771. <https://doi.org/10.3390/rs10111771>

References From the Supporting Information

- Bai, Y., & Cotrufo, M. F. (2022). Grassland soil carbon sequestration: Current understanding, challenges, and solutions. *Science*, 377(6606), 603–608. <https://doi.org/10.1126/science.abo2380>
- Bozdogan, H. (1987). Model selection and Akaike's Information Criterion (AIC): The general theory and its analytical extensions. *Psychometrika*, 52(3), 345–370. <https://doi.org/10.1007/bf02294361>
- Guillaume, T., Bragazza, L., Levasseur, C., Libohova, Z., & Sinaj, S. (2021). Long-term soil organic carbon dynamics in temperate cropland-grassland systems. *Agriculture, Ecosystems & Environment*, 305, e107184. <https://doi.org/10.1016/j.agee.2020.107184>
- Jones, M. B., & Donnelly, A. (2004). Carbon sequestration in temperate grassland ecosystems and the influence of management, climate and elevated CO₂. *New Phytologist*, 164(3), 423–439. <https://doi.org/10.1111/j.1469-8137.2004.01201.x>
- Krishnan, P., Meyers, T. P., Scott, R. L., Kennedy, L., & Heuer, M. (2012). Energy exchange and evapotranspiration over two temperate semi-arid grasslands in North America. *Agricultural and Forest Meteorology*, 153, 31–44. <https://doi.org/10.1016/j.agrformet.2011.09.017>
- Mensah, F., Schoenau, J. J., & Malhi, S. S. (2003). Soil carbon changes in cultivated and excavated land converted to grasses in east-central Saskatchewan. *Biogeochemistry*, 63(1), 85–92. <https://doi.org/10.1023/A:1023369500529>
- Myneni, R., Knyazikhin, Y., & Park, T. (2021). *MODIS/Terra Leaf Area Index/FPAR 8-Day L4 Global 500m SIN Grid V061*. NASA EOSDIS Land Processes DAAC. <https://doi.org/10.5067/MODIS/MCD15A3H.061>
- Shao, C., Chen, J., Chu, H., Laforzeza, R., Dong, G., Abraha, M., et al. (2017). Grassland productivity and carbon sequestration in Mongolian grasslands: The underlying mechanisms and nomadic implications. *Environmental Research*, 159, 124–134. <https://doi.org/10.1016/j.envres.2017.08.001>
- Zhang, Z., Zhou, Y., Ju, W., Chen, J., & Xiao, J. (2023). Accumulated soil moisture deficit better indicates the effect of soil water stress on light use efficiency of grasslands during drought years. *Agricultural and Forest Meteorology*, 329, e109276. <https://doi.org/10.1016/j.agrformet.2022.109276>